THE JOURNAL OF PHYSICAL CHEMISTRY A

Article

pubs.acs.org/JPCA

8-HaloBODIPYs and Their 8-(C, N, O, S) Substituted Analogues: Solvent Dependent UV−Vis Spectroscopy, Variable Temperature NMR, Crystal Structure Determination, and Quantum Chemical Calculations

Noël Boens,*[,†] Lina Wang,[†,∥] Volker Leen,[†] Peijia Yuan,[†,⊥] Bram Verbelen,[†] Wim Dehaen,[†] Mark Van der Auweraer,[†] Wim D. De Borggraeve,[†] Luc Van Meervelt,[†] Jeroen Jacobs,[†] David Beljonne,[‡] Claire Tonnelé,[‡] Roberto Lazzaroni,[‡] Maria J. Ruedas-Rama,[§] Angel Orte,[§] Luis Crovetto,[§] Eva M. Talavera,[§] and Jose M. Alvarez-Pez[§]

[†]Department of Chemistry, Katholieke Universiteit Leuven, Celestijnenlaan 200f − bus 02404, 3001 Leuven, Belgium

[‡]Laboratory for Chemistry of Novel Materials, Université de Mons, Place du Parc 20, 7000 Mons, Belgium

[§]Department of Physical Chemistry, University of Granada, Cartuja Campus, 18071 Granada, Spain

Supporting Information

ABSTRACT: The UV−vis electronic absorption and fluorescence emission properties of 8-halogenated (Cl, Br, I) difluoroboron dipyrrin (or 8-haloBODIPY) dyes and their 8-(C, N, O, S) substituted analogues are reported. The nature of the *meso*-substituent has a significant influence on the spectral band positions, the fluorescence quantum yields, and lifetimes. As a function of the solvent, the spectral maxima of all the investigated dyes are located within a limited wavelength range. The spectra of 8-haloBODIPYs display the narrow absorption and fluorescence emission bands and the generally quite small Stokes shifts characteristic of classic difluoroboron dipyrrins. Conversely, fluorophores with 8-phenylamino (**7**), 8-benzylamino (**8**), 8-methoxy (**9**), and 8-phenoxy (**10**) groups emit in the blue range of the visible spectrum and generally have larger Stokes shifts than common BODIPYs, whereas 8-(2-phenylethynyl)-BODIPY (**6**) has red-shifted spectra compared to ordinary BODIPY dyes. Fluorescence lifetimes for **6**, **8**, and **10** have been measured for a large set of solvents and the solvent effect on their absorption and emission maxima has been analyzed using the generalized Catalán solvent scales. Restricted rotation about the C8−N bond in **7** and **8** has been observed via temperature dependent ^{1}H NMR spectroscopy, whereas for **10** the rotation about the C8−O bond is not hindered. The crystal structure of **8** demonstrates that the short C8−N bond has a significant double character and that this N atom exhibits a trigonal planar geometry. The crystal structure of **10** shows a short C8−O bond and an intramolecular C−H···π interaction. Quantum-chemical calculations have been performed to assess the effect of the *meso*-substituent on the spectroscopic properties.

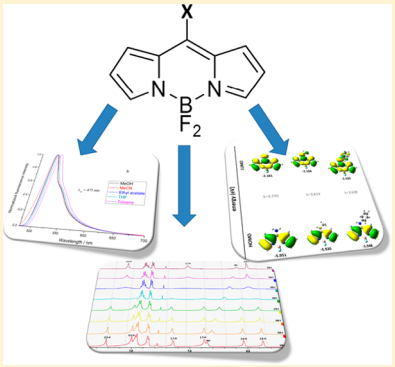

INTRODUCTION

Over the past decade, compounds derived from 4,4-difluoro-4-bora-3*a*,4*a*-diaza-*s*-indacene[1−3] have become very popular fluorescent dyes. The trade name BODIPY (acronym of *bo*ron *dipy*rrin or *bo*ron *dipy*rromethene),[4] has become the common name for this class of fluorophores. The success of BODIPY derivatives is attributable to their unique combination of spectroscopic and (photo)physical properties, such as the generally bright fluorescence with excitation/emission wavelengths in the visible region, narrow emission bandwidths with high peak intensities, robustness against light and chemicals, remarkable redox characteristics, resistance toward self-aggregation in solution, fluorescence lifetimes in the nanosecond range, and negligible triplet-state population. The other major reason for the attractiveness of these compounds is their vast potential for functionalization (at the pyrrole ring positions, the central 8- or *meso*-position, and the boron atom). A large number of functional groups can be introduced through well-documented postderivatizations of the BODIPY core, allowing a practically unlimited molecular structural modification and leading to sophisticated dyes with fine-tuned optical, (photo)physical, and chemical properties, for use as biological labels and probes, fluorescent indicators,[5,6] organic light emitting diodes, laser dyes,[7−9] potential photosensitizers in photodynamic therapy,[10] energy transfer cassettes,[9,11−22] and dye-sensitized solar cells.[9,23−29]

Recently, we described the synthesis of 8-halogenated (Cl, Br, I) difluoroboron dipyrrins, their substitution with (N, O, S) centered nucleophiles, and palladium catalyzed cross-couplings (Suzuki, Stille, Sonagashira).[30] In the present paper, we

Received: December 11, 2013
Revised: February 6, 2014
Published: February 6, 2014

Chart 1. Structure of the BODIPY Derivatives Studied

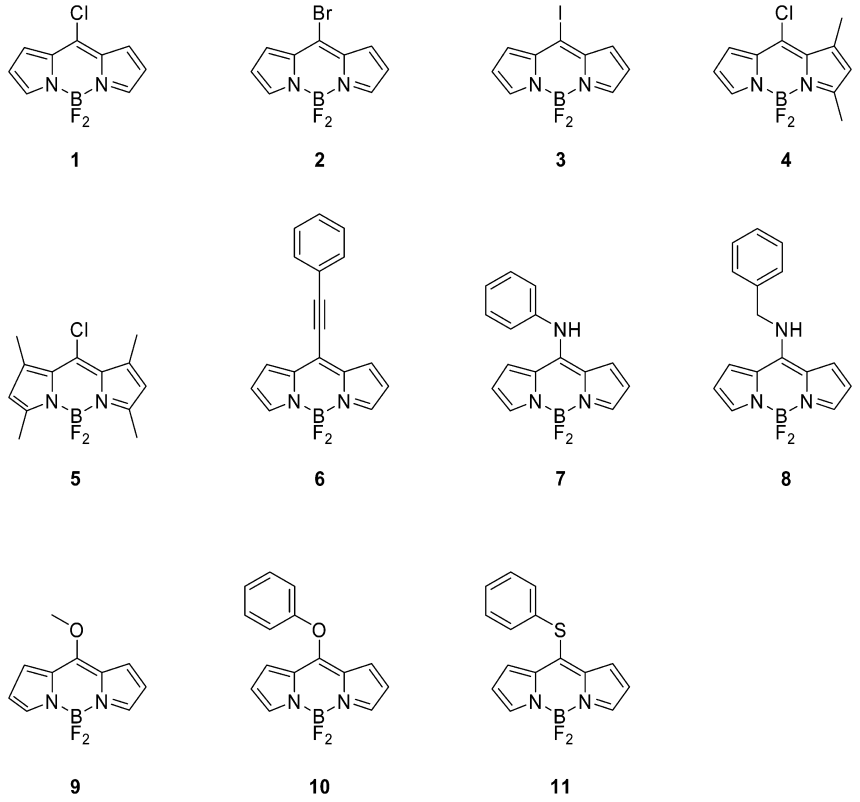

describe in detail the UV−vis spectroscopic properties of *meso*-halogenated (Cl, Br, I) 4,4-difluoro-4-bora-3*a*,4*a*-diaza-*s*-indacene dyes (**1**−**5**, Chart 1) and their 8-(C, N, O, S) substituted analogues (**6**−**11**, Chart 1). We investigated their spectroscopic and photophysical characteristics in solvents of widely varying properties by spectrophotometry and steady-state fluorometry. These experiments allowed us to determine the wavelengths of the spectral maxima [λ_{abs}(max), λ_{ex}(max), λ_{em}(max)], the full width at half-height of the maximum of the absorption (fwhm$_{abs}$) and fluorescence emission (fwhm$_{em}$) bands, the Stokes shifts [$\Delta = 1/\lambda_{abs}(max) - 1/\lambda_{em}(max)$], and the fluorescence quantum yields (Φ). We studied the effect of the nature of the *meso*-substituent and of the potential extension of the π-conjugation at the 8-position on the shifts of λ_{abs}(max) and λ_{em}(max) and on the Φ-values. Additionally, for **6** (with 8-C≡CPh), **8** (with 8-NHCH$_2$Ph), and **10** (with 8-OPh), we examined in detail the solvent effect on the position of the spectral maxima $\bar{\nu}_{abs} = 1/\lambda_{abs}(max)$ and $\bar{\nu}_{em} = 1/\lambda_{em}(max)$, employing the generalized treatment of the solvent effect based on a set of four empirical, mutually independent, complementary solvent scales (dipolarity, polarizability, acidity, and basicity of the medium).[31] Furthermore, the fluorescence lifetimes τ and the rate constants of fluorescence (k_f) and nonradiative decay (k_{nr}) were determined for **6**, **8**, and **10** for a large set of solvents. The restricted rotation about the C8−N bond in **7** and **8** and the unhindered rotation around the C8−O bond in **10** were evaluated using variable temperature ^{1}H NMR 600 MHz spectroscopy. X-ray diffraction was used to determine the crystal structure of **7**, **8**, and **10**. Finally, quantum-chemical calculations were performed to evaluate the influence of the *meso*-substituent on the spectroscopic properties of *meso*-substituted difluoroboron dipyrrins and the effect of the twist about the C8−N bond in 8-aminoBODIPYs on the energy was assessed via these calculations.

SYNTHESIS

Details of the synthesis (obtained products, reaction conditions, yields, product characterization) of the 8-haloBODIPYs investigated and their nucleophilic substitution and cross-coupling products can be found in ref 30. Chart 1 displays the structure of the dyes investigated. 8-(Benzylamino)-4,4-difluoro-4-bora-3*a*,4*a*-diaza-*s*-indacene (**8**) is a new product and was synthesized as in Scheme 1.

Scheme 1. Synthesis of 8 from 1

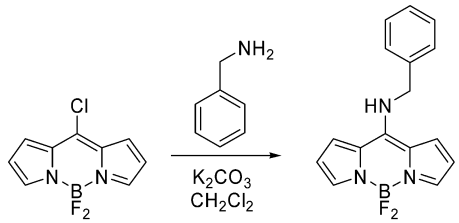

8-ChloroBODIPY (**1**) (22.6 mg, 0.1 mmol) was dissolved in dichloromethane (1 mL), and benzylamine (11 μL, 0.1 mmol) and K_2CO_3 (55 mg, 0.4 mmol) were added. The reaction mixture was purged with nitrogen and stirred at room temperature for 4 h. The crude mixture was poured out in diethyl ether, washed with a saturated aqueous NH_4Cl solution and brine, dried over $MgSO_4$, filtered, and evaporated to dryness. The residue was subsequently redissolved in CH_2Cl_2, and the solution was filtered over a silica pad. Product **8** was

dx.doi.org/10.1021/jp412132y | J. Phys. Chem. A 2014, 118, 1576−1594

Table 1. Spectroscopic and Photophysical Data of 8-Substituted BODIPYs as a Function of Solvent[a]

product	solvent	λ_{abs}(max)/nm	λ_{em}(max)/nm	$\Delta\bar{\nu}$/cm^{-1}	fwhm$_{abs}$/cm^{-1}	fwhm$_{em}$/cm^{-1}	Φ^b
1[c]	MeOH	500	511	431	939	1407	0.71 ± 0.02
	MeCN	499	511	471	1309	1491	0.69 ± 0.04
	EtOAc	501	513	467	909	1411	0.75 ± 0.01
	THF[g]	503	515	463	921	1388	0.72 ± 0.01
	toluene	507	520	493	898	1349	0.76 ± 0.01
2[c]	MeOH	501	514	505	908	1444	0.43 ± 0.02
	MeCN	500	513	507	1445	1510	0.51 ± 0.02
	EtOAc	502	515	503	879	1426	0.44 ± 0.03
	THF	504	517	499	880	1424	0.497 ± 0.008
	toluene	509	523	526	843	1399	0.55 ± 0.01
3[c]	MeOH	505	517	460	870	1540	0.12 ± 0.01
	EtOAc	506	517	420	896	1638	0.137 ± 0.005
	THF	507	519	456	860	1530	0.129 ± 0.005
	toluene	513	526	482	839	1530	0.147 ± 0.004
4[c]	MeOH	492	507	601	1364	1475	0.664 ± 0.007
	MeCN	490	507	684	1545	1464	0.667 ± 0.003
	EtOAc	493	508	599	1194	1435	0.712 ± 0.004
	THF	495	510	594	1155	1416	0.738 ± 0.005
	toluene	499	515	623	1015	1413	0.94 ± 0.01
5[c]	MeOH	499	514	585	1153	1826	0.450 ± 0.009
	MeCN	498	510	472	813	1430	0.38 ± 0.03
	EtOAc	500	511	431	754	1396	0.373 ± 0.009
	THF	502	513	427	774	1386	0.417 ± 0.008
	toluene	505	518	497	750	1288	0.62 ± 0.01
7[d]	MeOH	408	417	529	2385	2142	0.001 ± 0.001
	MeCN	407	421	817	2711	2137	0.001 ± 0.001
	EtOAc	412	419	405	2276	2030	0.002 ± 0.001
	THF	413	420	404	2233	2059	0.002 ± 0.001
	toluene	425	434	488	2073	2222	0.002 ± 0.001
9[e]	MeOH	441	484	2015	1718	1581	0.855 ± 0.004
	MeCN	438	483	2127	1817	1591	0.835 ± 0.005
	EtOAc	442	484	1963	1685	1573	0.859 ± 0.006
	THF	443	486	1997	1670	1575	0.852 ± 0.008
	toluene	449	490	1864	1453	1589	0.907 ± 0.009
11[f]	MeCN	492			2109		
	EtOAc	495			1976		
	THF	498			2069		
	toluene	501			1938		

[a]The solvents are listed from top to bottom according to increasing refractive index *n*. [b]Fluorescence quantum yield ± one standard uncertainty. [c]Φ determined vs fluorescein in 0.1 N NaOH (Φ_r = 0.90) as reference. [d]Φ determined vs coumarin 1 in ethanol (Φ_r = 0.64) as reference. [e]Φ determined vs acridine yellow G in methanol (Φ_r = 0.57) as reference. [f]Virtually nonfluorescent. In methanol, substitution of the 8-SPh group by methanol occurs, leading to bright fluorescence of **9** with concomitant spectral hypsochromic shifts. [g]THF = tetrahydrofuran.

obtained in 72% yield (21.5 mg) as a yellow crystalline solid after crystallization from a heptane/dichloromethane mixture by evaporation followed by washing with pentane. Mp: 138 °C. ^{1}H NMR ($CDCl_3$, 600 MHz): δ 7.72 (s, 1H), 7.52 (s, 1H), 7.48−7.40 (m, 3H), 7.37 (d, 2H, J = 6.90 Hz), 7.17 (s, 1H), 6.89 (s, 1H), 6.67 (s, 1H), 6.51 (s, 1H), 6.37 (s, 1H), 4.83 (d, 2H, J = 5.30 Hz) ppm. The number of proton signals is clearly much larger than what we normally would expect for a BODIPY. The reason is that the protons in both pyrrole rings are not equivalent, which gives rise to six signals instead of three for the pyrrole hydrogens. Because of the small coupling constants in pyrrolic dyes, the multiplicity of the pyrrole hydrogen signals is often unclear. This in combination with a broadening of the signals, due to the measurement temperature (room temperature) being close to the coalescence temperature, causes these signal to appear as singlets. Nevertheless, these signals do couple, as can be observed in a ^{1}H COSY NMR [Figure S7 (Supporting Information)]. The ^{1}H NMR spectrum of **8** is discussed more in detail in the section on "NMR Characterization of Meso-Substituted BODIPY Dyes" (see further). ^{13}C NMR [$(CD_3)_2SO$, 75 MHz]: δ 148.8, 135.9, 133.8, 131.0, 128.9, 127.6, 126.6, 125.2, 123.7, 121.6, 116.9, 114.4, 113.2, 49.3 ppm. In analogy with the ^{1}H NMR, the number of carbon signals exceeds the normally expected number for a BODIPY dye caused by the nonequivalence of the carbons in both pyrrole rings due to slow rotation around the C8−N bond (see further). MS (EI): 297 (M), 277 (M − HF). HRMS: Calculated for $C_{16}H_{14}BF_2N_3$: 297.12488, found 297.12770.

UV−VIS SPECTROSCOPIC AND PHOTOPHYSICAL PROPERTIES

The difluoroboron dipyrrin derivatives synthesized are strongly colored solids with a metallic luster that form intensely colored

Table 2. Spectroscopic and Photophysical Data of 6, 8, and 10 as a Function of Solvent[a]

product		solvent	λ_{abs}(max)/nm	λ_{em}(max)/nm	$\Delta\bar{\nu}$/cm^{-1}	fwhm$_{abs}$/cm^{-1}	fwhm$_{em}$/cm^{-1}	Φ[b]	τ[c]/ns	k_f[d]/10^8 s^{-1}	k_{nr}[d]/10^8 s^{-1}
6[e]	1	MeOH	539	553	470	975	1466	0.587 ± 0.006	7.16	0.82 ± 0.01	0.58 ± 0.01
	2	MeCN	537	553	539	1133	1551	0.624 ± 0.007	7.76	0.80 ± 0.01	0.48 ± 0.01
	3	Et_2O	541	555	466	879	1397	0.650 ± 0.004	7.80	0.83 ± 0.01	0.45 ± 0.01
	4	Me_2CO	539	554	502	1145	1539	0.55 ± 0.02	7.52	0.73 ± 0.03	0.60 ± 0.03
	5	EtOAc	540	553	435	941	1443	0.65 ± 0.02	7.46	0.87 ± 0.03	0.47 ± 0.03
	6	Bu_2O	543	556	431	837	1228	0.682 ± 0.005	7.21	0.95 ± 0.01	0.44 ± 0.01
	7	THF	543	556	431	961	1426	0.632 ± 0.007	6.91	0.91 ± 0.01	0.53 ± 0.01
	8	1,4-dioxane	544	558	461	921	1332	0.680 ± 0.005	6.92	0.98 ± 0.01	0.46 ± 0.01
	9	CH_2Cl_2	542	556	465	945	1339	0.658 ± 0.003	7.16	0.92 ± 0.01	0.48 ± 0.01
	10	$CHCl_3$	544	557	429	886	1206	0.686 ± 0.004	7.17	0.96 ± 0.01	0.44 ± 0.01
	11	toluene	547	562	488	937	1380	0.715 ± 0.006	6.88	1.04 ± 0.01	0.41 ± 0.01
	12	PhCl[h]	547	561	456	911	1347	0.715 ± 0.005	6.72	1.06 ± 0.01	0.42 ± 0.01
8[f]	1	MeOH	402	449	2604	2161	2967	0.081 ± 0.003	0.57	1.43 ± 0.05	16.15 ± 0.07
	2	MeCN	400	451	2827	2242	2887	0.164 ± 0.005	1.38	0.49 ± 0.02	2.48 ± 0.02
	3	Et_2O	410	454	2364	2020	2854	0.45 ± 0.07	4.82	0.9 ± 0.1	1.2 ± 0.1
	4	Me_2CO	403	449	2542	2219	2877	0.209 ± 0.005	1.46	1.43 ± 0.03	5.43 ± 0.04
	5	EtOAc	405	454	2665	2061	2957	0.60 ± 0.02	3.79	1.59 ± 0.05	1.05 ± 0.05
	6	2-propanol	406	446	2209	2003	2906	0.26 ± 0.01	1.67	1.53 ± 0.07	4.47 ± 0.08
	7	PrCN[h]	404	452	2629	2140	2870	0.48 ± 0.01	3.37	3.49 ± 0.07	3.76 ± 0.08
	8	Bu_2O	414	464	2603	1796	2813	0.61 ± 0.03	4.67	1.30 ± 0.06	0.84 ± 0.06
	9	1-butanol	406	447	2259	2061	2870	0.30 ± 0.02	2.07	1.5 ± 0.1	3.4 ± 0.1
	10	THF	406	453	2555	2175	2868	0.36 ± 0.02	2.61	1.39 ± 0.07	2.45 ± 0.07
	11	1-pentanol	407	448	2249	2051	2868	0.36 ± 0.02	2.44	1.47 ± 0.07	2.62 ± 0.07
	12	1,4-dioxane	409	454	2423	2087	2812	0.66 ± 0.03	4.16	1.58 ± 0.06	0.82 ± 0.06
	13	CH_2Cl_2	412	466	2813	1935	2810	0.52 ± 0.06	4.15	1.3 ± 0.1	1.2 ± 0.1
	14	c-C_6H_{12}[h]	422	469	2375	1736	2604	0.61 ± 0.02	4.90	1.24 ± 0.04	0.80 ± 0.04
	15	1-octanol	408	448	2188	1973	2888	0.51 ± 0.03	3.17	1.60 ± 0.09	1.55 ± 0.09
	16	$CHCl_3$	415	466	2637	2156	2802	0.46 ± 0.02	4.18	1.09 ± 0.04	1.30 ± 0.05
	17	c-$C_6H_{10}O$[h]	406	452	2507	2186	2829	0.35 ± 0.02	2.67	1.32 ± 0.09	2.43 ± 0.09
	18	CCl_4	422	468	2329	1736	2610	0.70 ± 0.03	4.32	1.61 ± 0.06	0.70 ± 0.06
	19	toluene	418	467	2510	1824	2662	0.75 ± 0.02	4.39	1.70 ± 0.04	0.58 ± 0.04
	20	PhCl[h]	416	465	2533	1833	2723	0.65 ± 0.02	4.09	1.58 ± 0.05	0.87 ± 0.05
10[g]	1	MeOH	443	487	2039	1906	1718	0.91 ± 0.01	6.30	1.44 ± 0.02	0.14 ± 0.02
	2	MeCN	451	493	1889	1719	1512	0.75 ± 0.02	5.56	1.35 ± 0.04	0.45 ± 0.04
	3	Et_2O	455	494	1735	1595	1475	0.93 ± 0.01	6.42	1.45 ± 0.02	0.11 ± 0.02
	4	Me_2CO	453	495	1873	1681	1540	0.89 ± 0.01	6.31	1.41 ± 0.02	0.17 ± 0.02
	5	EtOAc	454	493	1742	1630	1509	0.92 ± 0.02	6.25	1.47 ± 0.03	0.13 ± 0.03
	6	Bu_2O	457	495	1680	1570	1473	0.907 ± 0.008	5.87	1.55 ± 0.01	0.16 ± 0.01
	7	THF	456	495	1728	1685	1504	0.91 ± 0.02	5.77	1.58 ± 0.03	0.16 ± 0.04
	8	1,4-dioxane	457	497	1761	1645	1460	0.90 ± 0.01	5.58	1.61 ± 0.02	0.18 ± 0.02
	9	CH_2Cl_2	456	497	1809	1607	1468	0.88 ± 0.01	5.97	1.47 ± 0.02	0.20 ± 0.02
	10	$CHCl_3$	458	498	1754	1567	1430	0.92 ± 0.02	5.85	1.57 ± 0.03	0.14 ± 0.03
	11	toluene	460	500	1739	1572	1543	0.99 ± 0.01	5.29	1.87 ± 0.02	0.02 ± 0.02
	12	PhCl[h]	460	501	1779	1623	1526	0.87 ± 0.02	5.22	1.67 ± 0.04	0.25 ± 0.04

[a]The solvents are numbered according to increasing refractive index n. [b]Fluorescence quantum yield ± one standard uncertainty. [c]Fluorescence lifetime. The standard errors are obtained from the diagonal elements of the covariance matrix available from the global analysis fit of decay traces recorded at three different emission wavelengths λ_{em} and are between 11 and 13 ps for **6**, between 2 and 12 ps for **8**, and between 13 and 16 ps for **10**. λ_{ex} (**6**) = 532 nm, λ_{ex} (**8**) = 404 nm, λ_{ex} (**10**) = 440 nm. λ_{em} (**6**) = 555, 560, 565 nm; λ_{em} (**8**) = 450, 455, 460 nm; λ_{em} (**10**) = 490, 495, 500 nm. [d]The propagated errors are calculated using the standard uncertainty of Φ and the standard error of τ. [e]Φ determined vs rhodamine 6G in methanol (Φ_r = 0.86) as reference. [f]Φ determined vs quinine sulfate in 0.1 M H_2SO_4 (Φ_r = 0.54) as reference. [g]Φ determined vs acridine yellow G in methanol (Φ_r = 0.57) as reference. [h]PhCl = chlorobenzene, PrCN = butanenitrile, c-C_6H_{12} = cyclohexane, c-$C_6H_{10}O$ = cyclohexanone.

solutions with generally bright fluorescence upon irradiation. The variety of the groups at the 8-position of the BODIPY nucleus provides an outstanding opportunity for a detailed investigation of the spectroscopic and photophysical characteristics of these dyes as a function of the *meso*-substituent.

Although the shapes of the spectra of all the BODIPYs studied are comparable, their absorption [λ_{abs}(max)] and emission [λ_{em}(max)] maxima, Stokes shifts ($\Delta\bar{\nu}$), absorption (fwhm$_{abs}$) and emission (fwhm$_{em}$) bandwidths, and fluorescence quantum yields (Φ) may be quite different, depending on the type of *meso*-substituent (Cl, Br, I, C, N, O, S). Tables 1 and 2 compile the spectroscopic and photophysical data of all the dyes investigated as a function of solvent. In the following, we shall have a close look at the diversity of the spectroscopic and photophysical properties of the BODIPYs.

dx.doi.org/10.1021/jp412132y | J. Phys. Chem. A 2014, 118, 1576−1594

As a representative, illustrative example of the 8-halo-BODIPY derivatives, the visible electronic absorption and fluorescence emission spectra of 8-chloroBODIPY (**1**) dissolved in the solvents of Table 1 are shown in Figure 1.

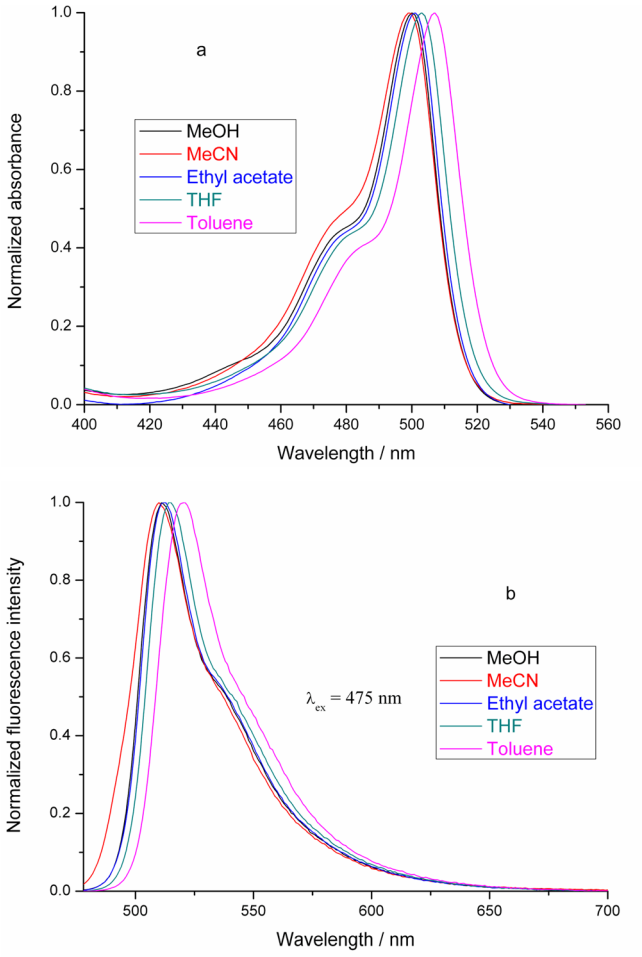

Figure 1. (a) Normalized, main $S_1 \leftarrow S_0$ visible absorption bands of **1** in the solvents indicated. (b) Corresponding normalized fluorescence emission spectra upon excitation at 475 nm.

Compound **1** displays the typical absorption features of classic difluoroboron dipyrrins in all solvents tested,[2,32−55] that is, a narrow, main absorption band with the maximum λ_{abs}(max) positioned within a very narrow range (499−507 nm) and which is slightly red-shifted with increasing solvent polarizability (from 499 nm in acetonitrile to 507 nm in toluene). This visible absorption band is assigned to the $S_1 \leftarrow S_0$ transition.

Derivative **1** also shows the characteristic emission features of difluoroboron dipyrromethene dyes, i.e., a narrow, slightly Stokes-shifted band of mirror image shape, which is red-shifted with increasing solvent polarizability [λ_{em}(max) moves from 511 nm in methanol and acetonitrile to 520 nm in toluene]. The other 8-haloBODIPYs (**2**−**5**, Chart 1) display absorption and emission spectra, which are of comparable shape as those of **1**. λ_{abs}(max) and λ_{em}(max) of these 8-haloBODIPYs are very alike (and consequently also the associated Stokes shifts $\Delta\bar{\nu}$) and follow the same trend vs the solvent (Table 1). The Stokes shifts for all the 8-haloBODIPYS are generally small (Table 1), in accordance with what is found for classic BODIPY derivatives.[2,32−55] The fwhm of the absorption spectra of **1**−**3** and **5** are quite small (usually <1000 cm^{-1}) and similar to what is found for *meso*-aryl substituted BODIPYs.[32] They increase somewhat upon increasing the solvent polarity. However, the absorption spectra of **4** are characterized by significantly larger $fwhm_{abs}$ which increases by 530 cm^{-1} from toluene to acetonitrile, which can be accounted for by the small ground-state dipole in **4** due to an asymmetric methyl substitution pattern. Contrary to what was found for the *meso*-aryl substituted BODIPYs,[32] the $fwhm_{em}$ of **1**−**5** are always larger, although slightly, than the $fwhm_{abs}$ and nearly independent of the solvent (with exception of some spurious results for **5** in methanol and for **3** in acetonitrile). Such a difference between the $fwhm_{abs}$ and $fwhm_{em}$ could suggest a decreased rigidity in the excited state. The fluorescence quantum yields Φ of **1**−**5** are moderately high and decrease predictably in the series **1** (8-Cl, Φ ∼ 0.7), **2** (8-Br, Φ ∼ 0.5), and **3** (8-I, Φ ∼ 0.1), due to the increasing heavy atom effect, which facilitates intersystem crossing. With the exception of **1**, the Φ-values of **2**−**5** decrease slightly, but consistently, upon increasing the solvent polarity. This decrease has also been observed for *meso*-aryl substituted BODIPYs and became more outspoken when the aryl moiety was substituted in *para*-position with a strong electron-releasing group.[32]

The nonemissive, 8-phenylthio substituted compound **11** (Chart 1, Table 1) has a somewhat blue-shifted and broader $S_1 \leftarrow S_0$ absorption band [λ_{abs}(max) varies from 492 nm in acetonitrile to 501 nm in toluene] compared to that of unsubstituted BODIPY (**15**, Chart 2),[56,57] common BODI-

Chart 2. Structure of the Additional BODIPY Derivatives Used in the Quantum-Chemical Calculations

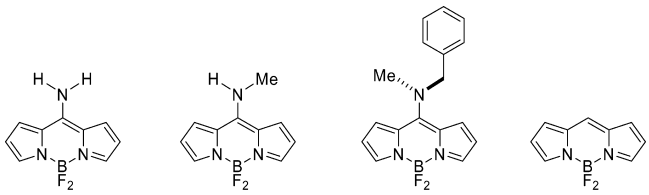

PYs,[2,32−55] and 8-chloroBODIPY (**1**), which can act as a benchmark for classic BODIPYs. In accordance with literature data,[58] 4,4-difluoro-8-(phenylamino)-4-bora-3*a*,4*a*-diaza-*s*-indacene (**7**, Chart 1, Table 1) is practically nonfluorescent (Φ ≤ 0.002) and has noticeably hypsochromically shifted λ_{abs}(max) and λ_{em}(max) in comparison to those of typical dipyrrins,[2,32−55] including the 8-haloBODIPYs. Other blue-emitting, 8-amino substituted dipyrromethene dyes have been described recently by Peña-Cabrera and co-workers.[59−62] The absorption [$fwhm_{abs}$ = (2.3 ± 0.2) × 10^3 cm^{-1}] and fluorescence [$fwhm_{em}$ = (2.12 ± 0.08) × 10^3 cm^{-1}] bands of **7** are much broader than those of common BODIPYs[32−41] and the present *meso*-haloBODIPYs. Blue-shifted λ_{abs}(max) and λ_{em}(max), and broader bandwidths $fwhm_{abs}$ [(2.0 ± 0.2) × 10^3 cm^{-1}] and $fwhm_{em}$ [(2.8 ± 0.1) × 10^3 cm^{-1}] in comparison to those of classic dipyrrins are also observed for **8** with an 8-benzylamino substituent [Chart 1, Table 2, Figure S1 (Supporting Information)]. However, in contrast to **7**, compound **8** is fluorescent; Φ increases from 0.08 in methanol up to 0.75 in toluene. Although for BODIPY derivatives with a *p*-anilino substituent at the *meso*-position a similar polarity dependence of Φ as for **8** was observed,[32] these

dx.doi.org/10.1021/jp412132y | J. Phys. Chem. A 2014, 118, 1576−1594

meso-p-anilino derivatives had lower fluorescence quantum yields and were nonfluorescent in polar solvents. Considering the lower ionization potential of an aromatic amine versus an aliphatic amine, the lower Φ-values of **7** and the *p*-anilino substituted *meso*-BODIPYs in ref 32 support our earlier hypothesis of acceleration of the internal conversion by coupling with an electron transfer state. Such internal conversion involving a low-lying charge transfer state close to S_1 was also suggested for perylene imides substituted by electron donor groups.[63] Even larger, solvent dependent changes in emission efficiency (Φ-values) have been reported for 8-isopropylaminoBODIPY and 8-isobutylaminoBODIPY.[62] Contrary to what was found for **7**, the blue shifts of **8** and other *meso*-amino substituted BODIPYs,[59,60] with respect to **1**, are more prominent for the absorption band than for the fluorescence band. For the solvents methanol, acetonitrile, ethyl acetate, THF (tetrahydrofuran), and toluene, the average blue shift ± one standard uncertainty of the absorption band of **8** with respect to **1** is $(4.7 \pm 0.3) \times 10^3$ cm^{-1}, whereas in emission it is only $(2.5 \pm 0.2) \times 10^3$ cm^{-1}. The average Stokes shift $\Delta\bar{\nu}$ ± one standard uncertainty for **8** in the 20 solvents of Table 2 is $(2.5 \pm 0.2) \times 10^3$ cm^{-1} and depends little upon solvent polarity. Comparison of compounds **7** and **8** with the previously investigated *meso-p*-anilino substituted BODIPYs[32] indicates that the behavior of the latter in apolar solvents resembles that of **7** whereas in more polar solvents it resembles that of **8**. 4,4-Difluoro-8-methoxy-4-bora-3*a*,4*a*-diaza-*s*-indacene (**9**, Chart 1, Table 1), the first reported 8-alkoxyBODIPY,[30] is highly fluorescent (Φ > 0.8) and also has blue-shifted λ_{abs}(max) and λ_{em}(max) in comparison to unsubstituted BODIPY (**15**, Chart 2)[56,57] and the usual dipyrromethenes,[32−55] but to a lesser degree than its 8-N substituted counterparts **7** and **8**. The absorption and emission bandwidths of **9** are broader [fwhm$_{abs}$ = $(1.7 \pm 0.1) \times 10^3$ cm^{-1} and fwhm$_{em}$ = $(1.58 \pm 0.01) \times 10^3$ cm^{-1}] than those of typical difluoroboron dipyrrins, but less broad than those of the *meso*-N derivatives.[32−41] In agreement with what was found for **8** and other reported *meso*-aminoBODIPYs,[59] the blue shifts of **9** with respect to **1** are larger for the absorption band than for the fluorescence band. For the five solvents of Table 1, the average blue shift of the absorption band of **9** with respect to **1** is $(2.67 \pm 0.09) \times 10^3$ cm^{-1}, whereas in emission it is only $(1.15 \pm 0.03) \times 10^3$ cm^{-1}, leading to a Stokes shift of $(2.0 \pm 0.1) \times 10^3$ cm^{-1}, which is quite large for a BODIPY dye. Similar observations are made for 4,4-difluoro-8-phenoxy-4-bora-3*a*,4*a*-diaza-*s*-indacene (**10**, Chart 1, Table 2), the first reported 8-aryloxyBODIPY.[30] For instance, the average Stokes shift $\Delta\bar{\nu}$ ± one standard uncertainty for **10** in the 12 solvents of Table 2 is $(1.8 \pm 0.1) \times 10^3$ cm^{-1}, somewhat smaller than for its 8-methoxy counterpart [$(2.0 \pm 0.1) \times 10^3$ cm^{-1}]. The fwhm$_{abs}$ and fwhm$_{em}$ values for **10** are $(1.65 \pm 0.09) \times 10^3$ cm^{-1} and $(1.51 \pm 0.07) \times 10^3$ cm^{-1}, respectively, and fwhm$_{abs}$ increases slightly upon increasing the solvent polarity. The electronic absorption and fluorescence emission spectra of **10** in a selection of solvents from Table 2 are displayed in Figure 2. In addition to the main absorption band (443−460 nm), assigned to the $S_1 \leftarrow S_0$ transition, a considerably weaker, broad absorption band can be observed in the UV spectral range (between 300 and 320 nm), which is attributed to the $S_2 \leftarrow S_0$ transition. Blue-shifted spectra have been described recently for 8-hydroxyBODIPY[64] and 8-alkoxy-BODIPYs[65,66] and 8-aryloxyBODIPYs.[66] High quantum yields combined with large Stokes shifts have been measured for these 8-OR substituted difluoroboron dipyrrins.[65,66] In addition, 8-alkoxyBODIPYs have good photostability, which is far superior to their 8-amino counterparts.[65] To finish, the 8-(2-phenylethynyl) substituent of **6** (Chart 1) causes remarkable bathochromic spectral shifts (Table 2). Indeed, introduction of the linear 8-C≡CPh group in **6** produces a red shift of ∼40 nm for λ_{abs}(max) and λ_{em}(max) in comparison to the the case for standard **1**, leading to small Stokes shifts [$(4.6 \pm 0.3) \times 10^2$ cm^{-1}], characteristic for common BODIPYs.[2,32−55] The red shifts indicate that the 2-phenylethynyl *meso*-substituent and the boradiazaindacene core form a conjugatively coupled π-system.[67] The quantum yields Φ of **6** are moderately high (0.6−0.7). The fwhm$_{abs}$ and fwhm$_{em}$ values are in line with those of common BODIPY compounds.[32−41] The absorption and fluorescence spectra of **6** are illustrated in Figure S2 (Supporting Information). In the literature, a series of *meso*-alkynylated ferrocenylBODIPYs have been synthesized recently using the Pd catalyzed Sonogashira cross-coupling reaction of 8-chloroBODIPY (**1**) with the corresponding ferrocenylethynes.[68] Three papers describe 8-alkynylBODIPYs obtained by the conventional route, i.e., condensation reaction of alkynyl acid chloride[69] or alkynyl aldehyde[67,70] with (substituted) pyrrole. Quantum-chemical simulations indicate that donor−acceptor 8-alkynylBODIPYs might have great potential as nonlinear optical chromophores.[71]

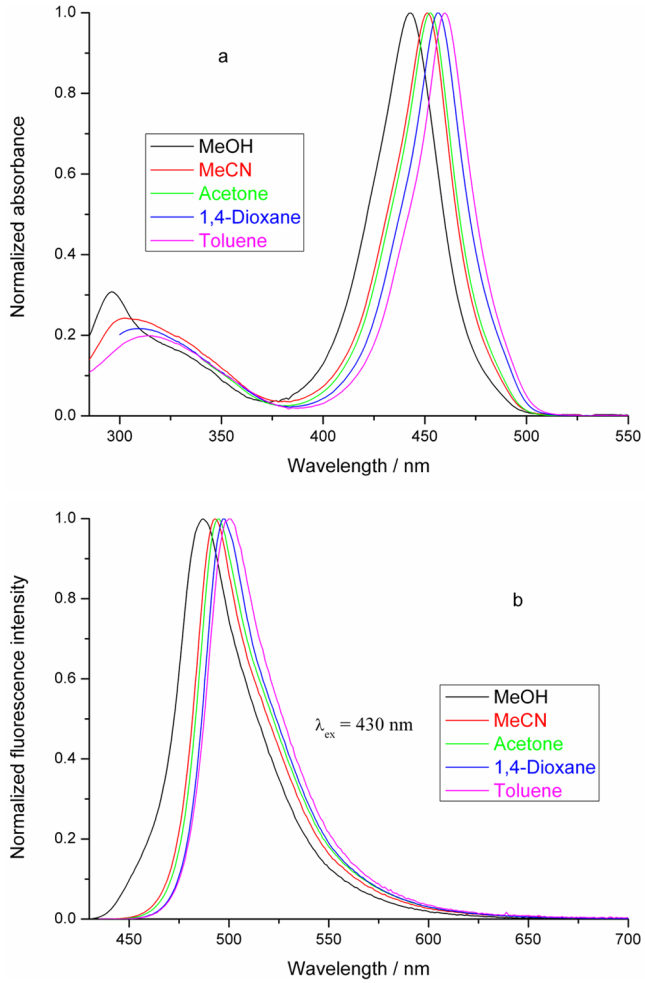

Figure 2. (a) Normalized, UV−vis absorption spectra of **10** in the solvents indicated. (b) Corresponding normalized fluorescence emission spectra upon excitation at 430 nm.

dx.doi.org/10.1021/jp412132y | J. Phys. Chem. A 2014, 118, 1576−1594

Table 3. λ_{abs}(max), ε_{max}, and Maximum Brightness Values for 6, 8, and 10 in Methanol, Acetonitrile, Ethyl Acetate, and THF[a]

compound		methanol	acetonitrile	ethyl acetate	THF
6	λ_{abs}(max)	539	537	540	543
	ε_{max}	$(62.2 \pm 0.6) \times 10^3$	$(8.0 \pm 0.1) \times 10^4$	$(30.4 \pm 0.3) \times 10^3$	$(43.5 \pm 0.3) \times 10^3$
	$\varepsilon_{max} \times \Phi$	$(36.5 \pm 0.5) \times 10^3$	$(50.1 \pm 0.9) \times 10^3$	$(19.7 \pm 0.8) \times 10^3$	$(27.5 \pm 0.4) \times 10^3$
8	λ_{abs}(max)	402	400	405	406
	ε_{max}	$(36.3 \pm 0.2) \times 10^3$	$(43.9 \pm 0.2) \times 10^3$	$(23.6 \pm 0.1) \times 10^3$	$(28.8 \pm 0.1) \times 10^3$
	$\varepsilon_{max} \times \Phi$	$(2.9 \pm 0.1) \times 10^3$	$(7.2 \pm 0.2) \times 10^3$	$(14.2 \pm 0.4) \times 10^3$	$(10.4 \pm 0.5) \times 10^3$
10	λ_{abs}(max)	443	451	454	456
	ε_{max}	$(42.9 \pm 0.3) \times 10^3$	$(60.0 \pm 0.5) \times 10^3$	$(241.2 \pm 0.8) \times 10^2$	$(34.7 \pm 0.2) \times 10^3$
	$\varepsilon_{max} \times \Phi$	$(38.8 \pm 0.6) \times 10^3$	$(45 \pm 1) \times 10^3$	$(22.2 \pm 0.4) \times 10^3$	$(31.7 \pm 0.8) \times 10^3$

[a]The maximum brightness is given by $\varepsilon_{max} \times \Phi$. λ_{abs}(max) is expressed in nm, ε_{max} and $\varepsilon_{max} \times \Phi$ in L mol^{-1} cm^{-1}.

Because the spectral maxima of all the 8-haloBODIPYs reported are very comparable to those of common difluoroboron dipyrrins, a comprehensive analysis of the influence of the solvent on $\overline{\nu}_{abs}$ and $\overline{\nu}_{em}$ is redundant. However, for the *meso*-(C, N, O) substituted **6**, **8**, and **10**, we shall describe in detail the solvatochromism of $\overline{\nu}_{abs}$ and $\overline{\nu}_{em}$.

Finally, it should be noted that the fluorescence excitation spectra of all the BODIPYs investigated match their absorption spectra.

Using the values of the molar absorption coefficient ε_{max} at λ_{abs}(max) and the fluorescence quantum yield Φ, the brightness (defined as the product $\varepsilon(\lambda_{abs}) \times \Phi$)[72] for a selection of dyes/solvents was exemplarily computed. The maximum values of the brightness for **6**, **8**, and **10** in methanol, acetonitrile, ethyl acetate, and THF are given in Table 3 and demonstrate that these compounds are generally bright fluorophores compared to oft-used fluorophores.[73] Dye **6** has the largest ε-values, followed by **10** and finally by **8**. For all three derivatives, the largest ε-values are found in acetonitrile, followed respectively by methanol, THF, and ethyl acetate. The brightness of **6** and **10** follows the same trend: highest in acetonitrile, followed by methanol, THF, and ethyl acetate. Conversely, the low Φ-values of **8** in methanol and acetonitrile reduce its brightness, so that the highest brightness values of **8** are found in ethyl acetate and THF.

To determine the fluorescence lifetimes (τ) and the rate constants for radiative ($k_f = \Phi/\tau$) and radiationless [$k_{nr} = (1 - \Phi)/\tau$] deactivation, fluorescence decay measurements for **6**, **8**, and **10** were performed using the single-photon timing technique with global analysis (Table 2).[74−76] In all cases, the fluorescence decay histograms collected at various emission wavelengths could be fitted globally with a single exponential function. Illustrative examples of fluorescence decay curves of **6**, **8**, and **10** and the curve fitting are shown in Figures S3−S5 (Supporting Information). For **6** the fluorescence lifetimes τ vary between 6.72 ns in chlorobenzene and 7.80 ns in diethyl ether, and for **10** between 5.22 ns in chlorobenzene and 6.42 ns in diethyl ether. The spread in τ-values is much larger for **8**: from 0.57 ns in methanol to 4.90 ns in cyclohexane. The radiative deactivation rate constant k_f is nearly solvent independent for each of the three dyes investigated: $(0.9 \pm 0.1) \times 10^8$ s^{-1} for **6**, $(1.5 \pm 0.6) \times 10^8$ s^{-1} for **8**, and $(1.5 \pm 0.1) \times 10^8$ s^{-1} for **10**. The nonradiative rate constant k_{nr} [$(0.48 \pm 0.06) \times 10^8$ s^{-1}] of **6** also is practically independent of the solvent.

SOLVATOCHROMISM

The solvent effect can be divided into specific (donor−acceptor and acid−base) interactions and nonspecific (arising from the solvent acting as a dielectric continuum) interactions. These interactions have been empirically parametrized by a sizable collection of solvent scales [see ref 31 and Supporting Information for an overview of solvent scales (or parameters) described in the literature]. The most comprehensive treatment of the influence of the solvent (based on a set of four empirical, complementary, mutually independent solvent scales) has recently been proposed by Catalán.[31] In this method, the polarizability and dipolarity of a particular solvent are characterized by the parameters SP[77] and SdP,[31] respectively, whereas acidity and basicity are described by the scales SA[78,79] and SB,[80] respectively (eq 1). The {SA, SB, SP, SdP} parameters for a large number of solvents can be found in ref 31. Mathematically, the solvent effect on the physicochemical observable y can be expressed by the multilinear eq 1:

$$y = y_0 + a_{SA}SA + b_{SB}SB + c_{SP}SP + d_{SdP}SdP \quad (1)$$

where y_0 denotes the physicochemical property of interest in the gas phase; a_{SA}, b_{SB}, c_{SP}, and d_{SdP} are regression coefficients that describe the sensitivity of the property y to the various solvent−solute interaction mechanisms; and {SA, SB, SP, SdP} are independent solvent parameters (indices) accounting for various types of solvent−solute interactions.

The spectroscopic observables y analyzed in this paper are the absorption maxima $\overline{\nu}_{abs} = 1/\lambda_{abs}$(max) and the emission maxima $\overline{\nu}_{em} = 1/\lambda_{em}$(max), both expressed in cm^{-1}.

Now we shall investigate the solvatochromic effect on the spectral maxima $\overline{\nu}_{abs}$ and $\overline{\nu}_{em}$ of 8-benzylaminoBODIPY **8**. λ_{abs}(max) varies 22 nm among the 20 solvents tested (from 400 nm in acetonitrile to 422 nm in cyclohexane and tetrachloromethane, corresponding to a shift of 1303 cm^{-1}), whereas a comparable 23 nm change of λ_{em}(max) is observed (from 446 nm in 2-propanol to 469 nm in cyclohexane, corresponding to a shift of 1100 cm^{-1}). Use of the Catalán solvent parameter set {SA, SB, SP, SdP} gives excellent fits to $\overline{\nu}_{abs}$ of **8** using r as goodness-of-fit criterion (eq 1 with r = 0.951, Table S1, Supporting Information). High-quality fits are also obtained for the multilinear analysis (eq 1) of $\overline{\nu}_{em}$ (r = 0.933, Table S1, Supporting Information).

The added benefit of the generalized (Catalán) treatment of the solvent effect is that it allows one to separate the relative contributions of dipolarity, polarizability, acidity, and basicity of the medium. Therefore, we utilized the new methodology to unravel which solvent property/properties is/are primarily responsible for the observed shifts of $\overline{\nu}_{abs}$. The large estimated d_{SdP}-value and its high precision (i.e., relatively small standard error) compared to {a_{SA}, b_{SB}, c_{SP}} are an indication that the change of $\overline{\nu}_{abs}$ may reflect principally a variation in dipolarity of the environment of the chromophore. In this respect,

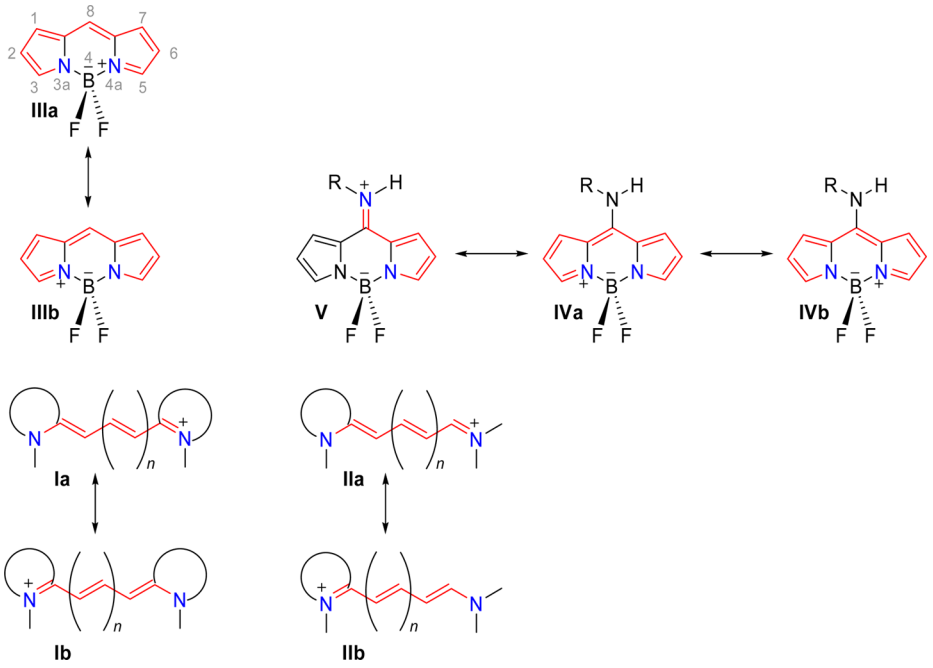

Figure 3. Closed chain cyanine (**I**) and hemicyanine (**II**) and the corresponding cyanine-like (**IVa** and **IVb**) and hemicyanine-like (**V**) structures of 8-aminoBODIPY. The cyanine-like structure of the BODIPY core is represented by **III**. For clarity, the polymethine chains linking two blue nitrogen atoms (one positive and one neutral) are shown in red. Although for **V** only one red polymethine chain is shown, actually there are two equivalent polymethine chains joining C8−N^+ with N3a (black) and N4a (red). Note that in **IVa** and **IVb**, one can distinguish additional hemicyanine-like structures (similar to **IIb**) in which C8−N and $N3a^+$ (in **IVa**) or $N4a^+$ (in **IVb**) are linked. The numbering of the BODIPY core (**IIIa**) is shown in gray.

compound **8** differs quite strongly from most BODIPYs investigated earlier,[32−41] where SP [or the related Bayliss function $f(n) = (n^2 - 1)/(2n^2 + 1)$] was the major cause for the solvent dependence of $\bar{\nu}_{abs}$. One should also note that the value of d_{SdP} is positive (Table S1, Supporting Information), indicating blue shifts with increasing SdP, whereas for other BODIPYs investigated earlier, d_{SdP}, if relevant, was negative. Such a positive value of d_{SdP} for $\bar{\nu}_{abs}$ suggests that the excited-state dipole moment is smaller than that of the ground state. Further supporting evidence that solvent dipolarity is the major factor influencing $\bar{\nu}_{abs}$ derives from the analyses of $\bar{\nu}_{abs}$ according to eq 1 in which one independent variable is omitted. As long as SdP (solvent dipolarity) is included in the analysis, the *r*-value remains high (r = 0.943, 0.929, and 0.914 for the analyses with {SB, SP, SdP}, {SA, SB, SdP}, and {SA, SP, SdP} as independent variables, respectively). Conversely, the analysis, in which SdP was left out, has the lowest *r*-value (0.674). That solvent dipolarity is not the sole factor affecting the position of the absorption maxima and that solvent basicity (SB) and polarizability (SP) (c_{SP} is quite large and as expected negative) are additional, although minor contributors, is confirmed by the analyses with {SB, SdP} and {SP, SdP} as independent variables, which both gave equally acceptable fits (r = 0.924 and 0.914, respectively; Table S1, Supporting Information). However, the key role of solvent dipolarity is obvious from the simple linear regressions of $\bar{\nu}_{abs}$ as a function of SA, SB, SP, and SdP only. Although the linear regression analysis vs SdP has r = 0.845, the three other linear regressions produce very low *r*-values (<0.595). That solvent acidity plays no role is clear from the comparison of the *r*-values of the multilinear fits with {SB, SP, SdP} (r = 0.943) and with {SA, SB, SP, SdP} (r = 0.951) as independent variables: inclusion of SA in the analysis has an insignificant effect. To summarize, solvent dipolarity is the major factor influencing the position of $\bar{\nu}_{abs}$ of **8** with solvent basicity and polarizability as minor contributors.

Which solvent characteristics principally account for the shifts of $\bar{\nu}_{em}$? The relatively large estimates of b_{SB} and d_{SdP} and their high precision (i.e., comparatively small standard errors) in relation to {a_{SA}, c_{SP}} point to solvent dipolarity and basicity as key factors determining $\bar{\nu}_{em}$. If either SB or SdP was left out as an independent variable in the analyses of $\bar{\nu}_{em}$ according to eq 1 (that is, with {SA, SP, SdP} and {SA, SB, SP}, respectively), low *r*-values (0.805 and 0.850, respectively) were found, implying the importance of these solvent parameters. Further evidence for SB and SdP as key parameters derives from the six possible analyses with two solvent scales as independent variables: the analysis with {SB, SdP} yields the best fit as judged by the *r*-value (0.924, Table S1, Supporting Information), which is only fractionally lower than that for the full analysis according to eq 1 (r = 0.933). As found for $\bar{\nu}_{abs}$, solvent acidity does not influence the position of $\bar{\nu}_{em}$: the fits with {SA, SB, SP, SdP} and {SB, SP, SdP} as independent variables give near-identical parameter estimates and *r*-values (Table S1, Supporting Information). To sum up, solvent dipolarity and basicity are the crucial factors that have an effect on $\bar{\nu}_{em}$ of **8**. The dependence of $\bar{\nu}_{em}$ upon solvent dipolar polarity (SdP) rather than solvent polarizability (SP) differs from what was observed for previously reported BODIPYs.[32−41] Furthermore, one should note that the slope obtained for SP (c_{SP}) has the same (negative) sign as observed for other BODIPYs.[38] However, the slope obtained for SdP (d_{SdP}) is positive in contrast to the negative slope obtained for other BODIPYs with electron donor substituents.[38] The destabilization of the excited state of **8** in polar, basic solvents (as implied by the positive values of d_{SdP} and b_{SB} for both $\bar{\nu}_{abs}$

dx.doi.org/10.1021/jp412132y | J. Phys. Chem. A 2014, 118, 1576−1594

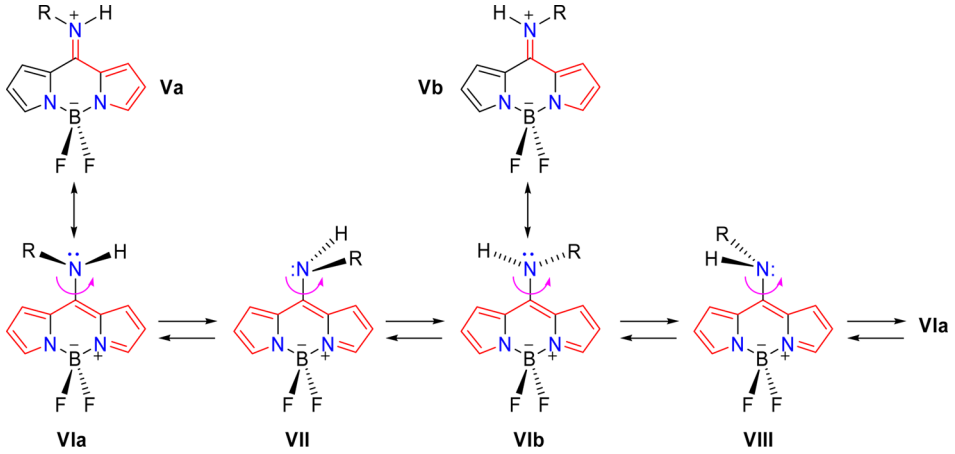

Figure 4. Rotation about C8−N bond inducing asymmetry in the molecule. Cyanine-like (in **VI**−**VIII**) and hemicyanine-like (in **V**) structures are indicated in red.

and $\bar{\nu}_{em}$) can be explained by the significant contribution of hemicyanine-like, polar Lewis structure **V** (R = $-CH_2Ph$, Figures 3 and 4) with an acidic iminium ion to the ground state of **8**, which decreases upon excitation in favor of the less dipolar cyanine Lewis structure **IV**.

As shown in Table 2, the influence of the solvent on λ_{abs}(max) (or $\bar{\nu}_{abs}$) and λ_{em}(max) (or $\bar{\nu}_{em}$) of 8-C≡CPh (**6**) and 8-OPh (**10**) substituted difluoroboron dipyrrins is much smaller than for **8**. For instance, λ_{abs}(max) of **6** moves only 10 nm among the 12 solvents tested (from 537 nm in acetonitrile to 547 nm in toluene and chlorobenzene, corresponding to a shift of 340 cm^{-1}), whereas a similar 9 nm change of λ_{em}(max) is observed (from 553 nm in methanol and acetonitrile to 562 nm in toluene, corresponding to a 290 cm^{-1} shift). For **10**, the solvatochromic shifts are somewhat larger: λ_{abs}(max) moves 17 nm (from 443 nm in methanol to 460 nm in toluene and chlorobenzene, corresponding to an 834 cm^{-1} shift). A 14 nm change of λ_{em}(max) is observed (from 487 nm in methanol to 501 nm in chlorobenzene, corresponding to a shift of 574 cm^{-1}). The Catalán analysis of the solvatochromic shifts of $\bar{\nu}_{abs}$ and $\bar{\nu}_{em}$ of **6** and **10** (Table 2), for which 12 solvents were tested, are described and discussed in the Supporting Information. Comparison of the analyses of the $\bar{\nu}_{abs}$ and $\bar{\nu}_{em}$ data for **6** and **10** (Supporting Information) with that for **8**, shows much smaller values of d_{SdP} and b_{SB}, whereas similar values are found for c_{SP}. These results are typical for BODIPYs without strong electron-donating substuents.[32−41]

HEMICYANINE VS CYANINE IN 8-AMINOBODIPYS

Cyanines are conjugated compounds where two nitrogen atoms, one of which is positively charged, are joined by a polymethine chain (drawn in red in Figure 3) with an odd number of carbon atoms.[81−86] In (closed chain) cyanines **I** both nitrogens are part of a heteroaromatic moiety. The core BODIPY structure **III** is similar to that of cyanine **I** (Figure 3). If only one of the N atoms is part of a heterocycle (e.g., **II**), the compound is termed a hemicyanine.[84,85,87] 8-AminoBODIPYs can be represented by cyanine-like Lewis structures **IV** (similar to **I**) and/or hemicyanine-like Lewis structure **V** (similar to **IIa**), dependent on the twisting ability of the 8-amino group (see further).

8-AminoBODIPYs are characterized by unusual fluorescence in the blue-edge spectral region.[58−62] Quantum chemical DFT calculations presented here (see further) and in the literature[59−61] indicate that the observed hypsochromic spectral shifts compared to those of common BODIPY dyes are due to a net destabilization of the LUMO state whereas the HOMO remains unaltered by the presence of a *meso*-amino group. X-ray diffraction data of 8-phenylaminoBODIPY (**7**) has shown coplanarity of the boradiazaindacene ring system with the 8-amino group.[58] The C8−N bond length (1.23−1.34 Å) is close to that of a C=N double bond, so it was proposed that the structure of the ground state of **7** is best described by a hemicyanine-like Lewis structure **V** (Figures 3 and 4 with R = Ph).[58] This also corroborates our analysis of the solvent effect on the spectra of **8**, which suggested a major contribution of the dipolar hemicyanine Lewis structure to the ground state, which upon excitation decreased in favor of the less dipolar cyanine Lewis structure. This dipolar ground state also accounts for the $fwmh_{em}$ of **8** being larger than $fwmh_{abs}$, in contrast to what is found for other BODIPYs. This means that the chromophore of **8** should be called a hemicyanine rather than a *meso*-amino substituted monomethine cyanine, although the latter is also expected to have hypsochromically shifted absorption and emission.[81,87] Further research by Peña-Cabrera and co-workers on 8-NHR substituted BODIPY analogues without steric hindrance [with R = H,[60] Me,[60] prop-2-ynyl (propargyl),[59] prop-2-enyl (allyl)[60]] and with steric constraints (with R = tBu,[61] iPr,[62] iBu[62] or with methyl groups at the 1,7-positions)[61] indicated the essential role of the 8-amino twisting ability. When a coplanar arrangement of the π-system of the BODIPY core with the p-orbital amino group is feasible, a hemicyanine-like delocalized π-system **V** with sp^2 hybridized N (i.e., trigonal planar N, Figures 3 and 4) can be formed. If a near-coplanar conformation (such as **VI** in Figure 4) is possible, the lone electron pair of the 8-amino group is still in the right orientation for efficient electronic coupling with the π-system of the BODIPY core (Figure 4). Once the N lone electron pair is delocalized over the boron dipyrrin ring system, the hemicyanine-like structure **V** with a concomitant, reduced C8—N bond distance (Figures 3 and 4) would contribute predominantly to the overall structure of the ground state of 8-aminoBODIPYs. A cross-conjugated Lewis structure **V** with shorter polymethine chains than the cyanine-like Lewis structures **IV** (Figure 3) or **VI**−**VIII** (Figure 4) as well a different stability of the Lewis structures **IV** and **V** led to significant hypsochromic shifts of the absorption and fluorescence emission bands. The conformational model

dx.doi.org/10.1021/jp412132y | J. Phys. Chem. A 2014, 118, 1576−1594

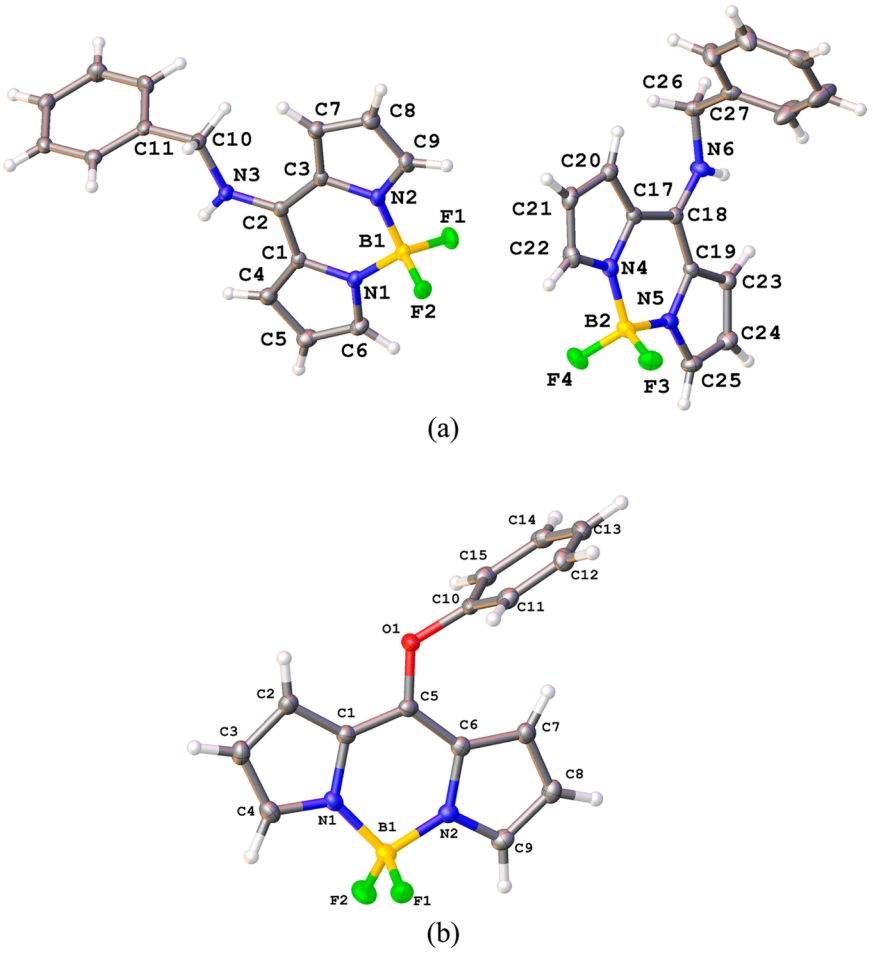

Figure 5. Molecular structure of **8** (a) and **10** (b). Displacement ellipsoids are drawn at the 50% probability level.

presented in Figure 4 also accounts for the largely coplanar arrangement of the BODIPY core and the amino plane (i.e., small dihedral angle between BODIPY core and C8—NR plane) in several 8-NHR-BODIPYs for which crystal structural data are available (R = Ph,[58] prop-2-ynyl,[59] iPr,[62] iBu[62]). The C8—N bond lengths for 8-isopropylaminoBODIPY and 8-isobutylaminoBODIPY are in the range 1.31−1.35 Å,[62] typical for bonds intermediate between a C—N and C═N bond, hinting at the important (although less than in the coplanar **8**) contribution of hemicyanine-like Lewis structure **V** to the overall structure of these compounds. Conversely, boron dipyrrins, in which a coplanar disposition of the BODIPY ring and the C8—NR group cannot be achieved, should behave more like a cyanine-like BODIPY system **IV** (Figure 3) with bathochromically shifted absorption and fluorescence emission bands. Bulky *meso*-(di)alkylamino substituents would lead to an energetically unfavorable hemicyanine-like **V** (Figures 3 and 4) because the (near)planar conformations **VI** (Figure 4) required for lone electron pair delocalization are impossible for large groups with steric repulsion.

CRYSTAL STRUCTURE DETERMINATION OF 8 AND 10

The molecular and crystal structures of three BODIPY derivatives (**7**, **8**, and **10**) were determined by X-ray diffraction. The crystal structure of two polymorphs of **7** has been reported by Goud et al.[58] Different crystallization conditions (diffusion of pentane into a dichloromethane solution versus hexane/chloroform and chloroform used by Goud et al.) did not result in a different polymorph.

A view of the molecular structures of the two molecules (A, left, and B, right) in the asymmetric unit of **8** is shown in Figure 5a. Note that the numbering of the atoms in the crystal structures is different from the IUPAC numbering. In both cases the BODIPY core ring is near-planar with a maximal deviation from planarity for molecule A of +0.041(2) Å for atom B1 and −0.069(2) Å for atom B2 for molecule B. The dihedral angle between the two pyrrole rings is 0.97(10)° (molecule A) and 5.16(11)° (molecule B). The *meso*-substituent is situated in the same plane (deviation of −0.037(2) Å for atom N3 in molecule A and −0.045(1) Å for atom N6 in molecule B). The dihedral angle between the BODIPY core and the NR_2 plane is 3.14(10)° (molecule A) and 2.65(11)° (molecule B). Both molecules differ in the orientation of the phenyl substituent as illustrated by the torsion angles C2−N3−C10−C11 of 160.43(16)° for molecule A and C18−N6−C26−C27 of 81.0(2)° for molecule B. The phenyl group makes an angle of 77.72(7)° (molecule A) and 79.93(9)° (molecule B) with the plane of the 12-membered ring. Bond lengths C2−N3 (1.331(3) Å) and C18−N6 (1.326(2) Å) are short, indicating their double bond character. The crystal packing of **8** is mainly determined by C−H···π and C/N−H···F interactions.

The molecular structure of **10** is shown in Figure 5b. Again, the numbering of the atoms in the crystal structure is different from the IUPAC numbering. The BODIPY core ring is close to

dx.doi.org/10.1021/jp412132y | J. Phys. Chem. A 2014, 118, 1576−1594

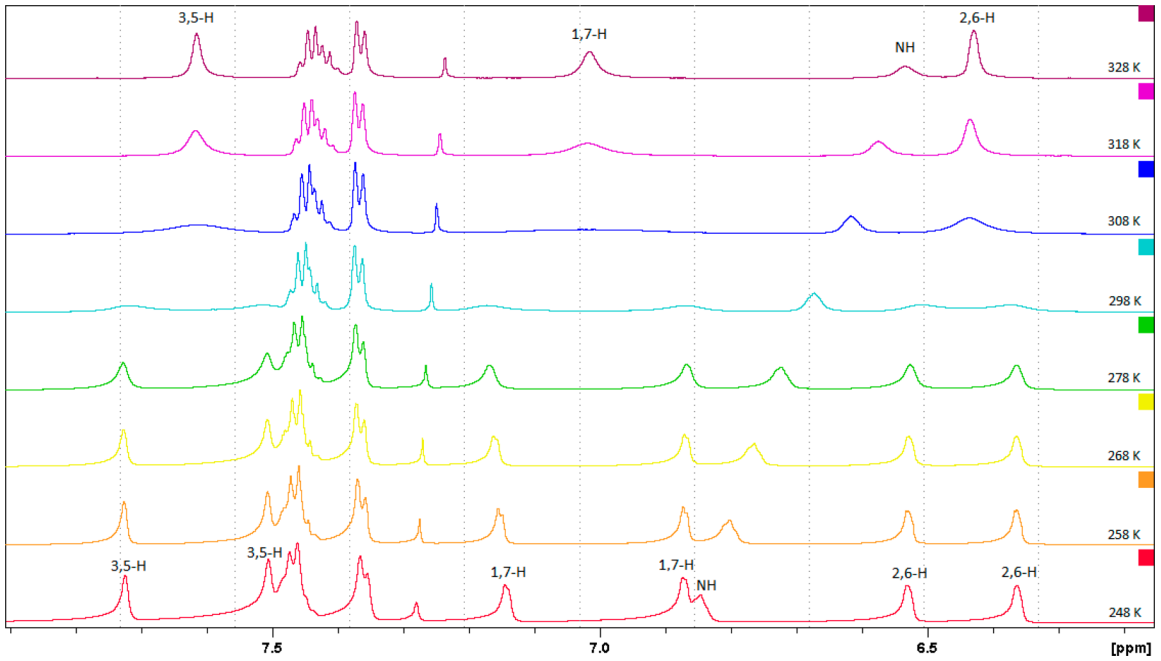

Figure 6. Aromatic region of the temperature dependent ^{1}H NMR spectra of **8** measured in $CDCl_3$ at 600 MHz from −25 °C (bottom) to +55 °C (top).

planar with a slightly higher maximal deviation from planarity of 0.152(2) Å for atom B1. The dihedral angle between both pyrrole rings is 4.59(10)°. The *meso*-substituent O1 deviates 0.019(1) Å from the core ring. The torsion angle C6−C5−O1−C10 of −7.6(2)° keeps atom C10 almost in the BODIPY plane (deviation is 0.160(2) Å). The dihedral angle between the best planes through the BODIPY core and the phenyl ring is 85.71(7)°. The orientation of the phenyl ring is such that an intramolecular H7···π interaction (2.718(19) Å) is possible. The C5−O1 bond length (1.3457(19) Å is shortened, reflecting the partial double bond character. The crystal packing of **10** is determined by π···π, C−H···π, and C−H···F interactions. Further crystallographic details are given in Table S3 (Supporting Information).

NMR CHARACTERIZATION OF *MESO*-SUBSTITUTED BODIPY DYES

A literature study of 8-*sec*-aminoBODIPY dyes reveals that these derivatives display different ^{1}H NMR spectra depending on the solvent used.[59,61,62] In general, polar solvents like CD_3CN result in six nonequivalent pyrrole hydrogen signals, whereas less polar solvents like $CDCl_3$ produce spectra consisting of three pyrrole H peaks. It was suggested that in the more polar solvents conformations **VIa** and **VIb** (Figure 4), in which the *meso*-N-substituents are almost coplanar with the dipyrrin ring, could be formed by rotation about the C8−N bond. However, no experimental evidence for such a restricted rotation was presented. Conformations **VI** allow the N-lone electron pair to be delocalized into the π-system of the BODIPY core with the resultant hemicyanine-like **V** (Figures 3 and 4), which is stabilized by polar solvents, being an important contributor to the overall structure of the ground state. The higher double bond character of the C8−N bond in hemicyanine-like **V** (as is evident from the crystal structure determinations and the solvent dependence of $\overline{\nu}_{abs}$ and $\overline{\nu}_{em}$) leads to a hindered rotation around this bond and a corresponding nonequivalent environment for the BODIPY pyrrole hydrogens. The extra signals in polar solvents are thus accounted for by contribution of the delocalized hemicyanine-like Lewis structure **V** to the total structure.

By using variable temperature ^{1}H NMR spectroscopy, Pannell and co-workers recently presented experimental evidence for restricted rotation about the C8−N bond in 8-isopropylaminoBODIPY and 8-isobutylaminoBODIPY in $CDCl_3$ solution.[62] The ^{1}H NMR spectra in $CDCl_3$ at 5 °C for these compounds exhibited six sharp peaks in the aromatic region, implying that the isopropyl and isobutyl groups, together with the delocalization of the N-lone electron pair, induce enough steric hindrance to give rise to a restricted rotation about the C8−N bond, thus reflecting an equilibrium between the conformations **VI**−**VIII**, as illustrated in Figure 4. This was confirmed by variable temperature ^{1}H NMR in $CDCl_3$: progressively raising the temperature resulted in a broadening and final coalescing of the 6 resonances into 3 singlets, as expected for the now rapid rotation about the C8−N bond. Activation energies of 59.2 and 62.9 kJ/mol were found for 8-isopropylaminoBODIPY and 8-isobutylamino-BODIPY, respectively.[62] Such values of the activation energies are reasonable for molecules where coalescence occurs close to room temperature. As expected, symmetrical BODIPYs (e.g., 8-aminoBODIPY and 8-diethylaminoBODIPY) displayed equivalent signals for the pyrrole ring protons in ^{1}H NMR because the hemicyanine-like Lewis structure **V** is symmetrical. Hence, only three resonances were observed in the ^{1}H NMR spectrum, regardless of solvent.[60,62] Conversely, because of steric constraints, 8-*tert*-butylaminoBODIPY and 8-propargylamino-1,3,5,7-tetramethylBODIPY[61] cannot achieve the coplanar conformations **VI**. As a result, the pyrrole protons become equivalent, giving rise to only three resonances in ^{1}H NMR at temperatures where the rate of interconversions between **VI**, **VII**, and **VIII** is fast compared to the difference in Larmor frequency.

Contrary to literature examples, the ^{1}H NMR spectra at room temperature of 8-benzylaminoBODIPY **8** in $CDCl_3$

measured at 600 MHz gave six separate (though very broad) peaks for the pyrrole hydrogens. The broadness of the signals could be accounted for if the coalescence temperature is close to room temperature. This was tested by measuring the ^{1}H NMR at different temperatures ranging from −25 to +55 °C (Figure 6). Lowering the temperature sharpened the peaks, transforming the spectra into that of an asymmetrical BODIPY as typically measured in polar solvents (Figure S8, Supporting Information). The polar solvents will increase the contribution of the more dipolar Lewis structures **V** in comparison to **VI** and hence increase the double bond character of the C8−N bond. Increasing the temperature causes the six peaks to coalesce into three peaks, signaling a symmetrical molecule on the NMR time scale due to a faster rotation about the C8−N bond.

Using the coalescence temperature (T_c) and the maximum separation between the signals of the exchanging nuclei ($\Delta\nu$) for each set of peaks, the free enthalpy of activation at the coalescence temperature ($\Delta G_c^{\neq}$) can be approximated using Eyring's equation (eq 2),[88]

$$\Delta G_c^{\ddagger} = 19.14 T_c \left(10.32 + \log\left(\frac{T_c}{k_c}\right)\right) \text{J mol}^{-1} \quad (2)$$

where k_c ($=\pi\Delta\nu/\sqrt{2}$) is the rate constant for the exchange process at T_c (Table 4). Taking the average of the free enthalpy of activation for the three sets of peaks, gives a rotational free enthalpy barrier, $\Delta G^{\ddagger}$, of 61.0 kJ/mol for the C8−N bond of the 8-benzylamino compound **8**. This value is consistent with other 8-amino BODIPY compounds previously reported in the literature and assuming a small value of $\Delta S^{\ddagger}$.[62]

Table 4. Rate Constants and Free Enthalpy of Activation at the Coalescence Temperature T_c for 8

peak	$\Delta\nu$/Hz	k_c/s^{-1}	T_c/K	$\Delta G_c^{\ddagger}$/kJ mol^{-1}
1,7-H	163	362	308	60.4
2,6-H	100	222	308	61.7
3,5-H	131	292	308	61.0

The ^{1}H NMR spectra of 8-(*N*-phenyl)BODIPY **7** in $CDCl_3$ at 600 MHz consisted of three pyrrole H peaks at room temperature, indicative of a symmetrical molecule or a fast interconversion between two asymmetrical conformations **VI**. In an effort to determine the rotational energy barrier of the C8−N bond of this dye, ^{1}H NMR measurements were taken at lower temperatures (Figure S6, Supporting Information). At −65 °C, the spectra correspond to an asymmetrical BODIPY dye. However, in contrast to **8**, the hydrogens at the 3,5-positions did not give rise to two separate peaks and remained as one signal, probably because these hydrogens are furthest away from the C8−N bond. Meanwhile, the 1,7-hydrogens, closest to the C8−N bond, display a very large separation of 1.35 ppm compared to 0.21 ppm for the 2,6-hydrogens (Table S2, Supporting Information). One should note that the separation of the signals of the 1,7-hydrogens is much larger than in **8** where it amounts to only 0.3 ppm. This larger separation can be related to the anisotropic effect of the phenyl moiety.

Calculating the free enthalpy of activation at the coalescence temperature T_c for **7** results in an average value of 43.8 kJ/mol (Table S2, Supporting Information). This value is lower than that for **8**, pointing to a less hindered rotation around the C8−N bond and hence a lower double bond character of this bond. Because N−Ph in **7** is less electron releasing than N−CH_2Ph in **8** due to delocalization of the lone electron pair into the phenyl ring, one can expect less double bond character for the C8−N bond in **7** than in **8**. The smaller contribution of this hemicyanine-like Lewis structure **V** corresponds also with the smaller blue shift of **7** compared to **8** [λ_{abs}(max) in toluene being at 425 and 418 nm, respectively]. On the basis of the X-ray diffraction data of **7** and **8** (see above) and the DFT calculations (see further), the slow rotation corresponds for **7** and **8** to interconversion between conformations **VIa** and **VIb**.

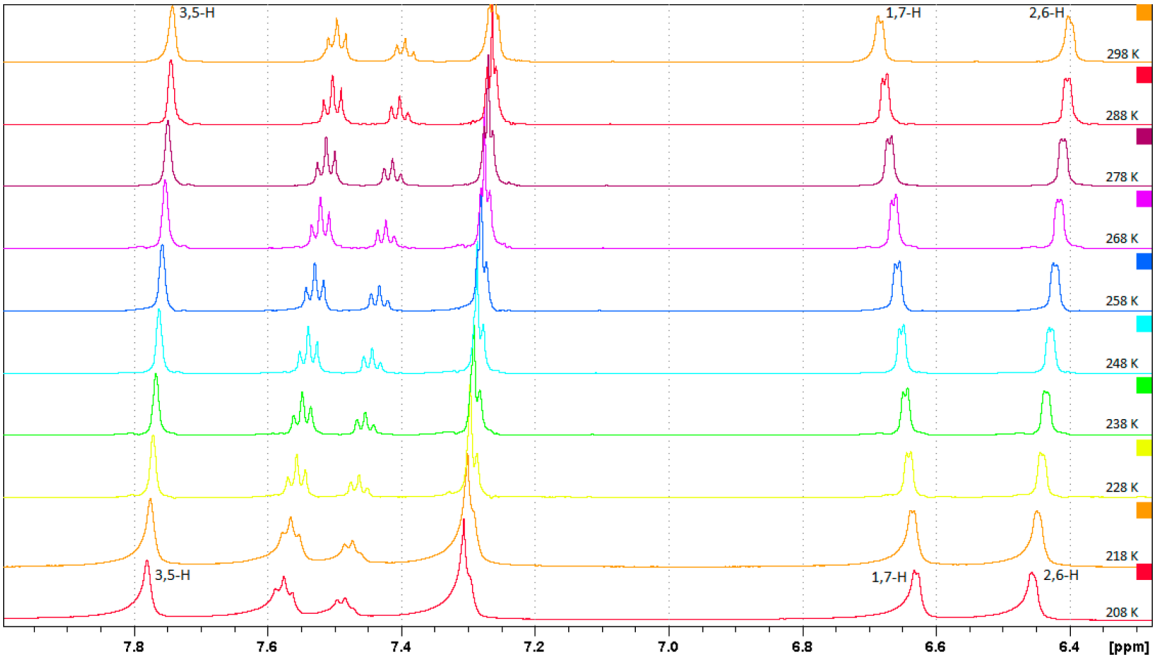

Figure 7. Aromatic region of the ^{1}H NMR spectra of **10** measured in $CDCl_3$ at 600 MHz as a function of temperature from +25 °C (top) to −65 °C (bottom).

dx.doi.org/10.1021/jp412132y | J. Phys. Chem. A 2014, 118, 1576−1594

Lastly, 8-(O-phenyl)BODIPY **10** was examined to investigate if a similar double bond character and hindered rotation is present in the C8−O bond. Even at −65 °C, the ^{1}H NMR in $CDCl_3$ at 600 MHz consisted of three pyrrole hydrogen signals (Figure 7). Hence, one can conclude that the rotational barrier around the C8−O bond in **10** is lower than the barrier of the C8−N bond in 8-(*N*-phenyl)-BODIPY **7**. This nearly unhindered rotation about the C8−O bond in the temperature range from +25 to −65 °C is indicative of the lower double bond character of this bond and guarantees that the conformations **X** and **XI** (Figure 8) can be easily populated

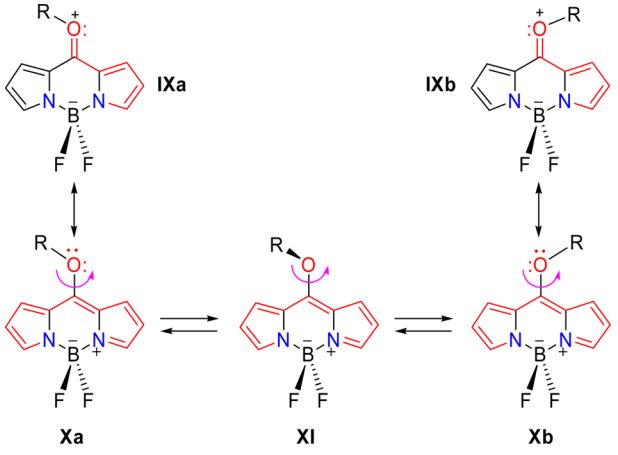

Figure 8. Rotation about the C8−O bond. Cyanine-like (in **X**, **XI**) and merocyanine-like (in **IX**) Lewis structures are indicated in red.

and are separated by a small energy barrier. From conformations **X**, with coplanar arrangement of the BODIPY core and the C8−O−Ph group, delocalization of one O-lone electron pair over the π-system producing the merocyanine-like Lewis structures **IX** can occur. This leads to an increased sp^2 character of the hybridization of O and a shortened C−O bond (see crystal structure) in **10**. Indeed, in conformations **X**, one lone electron pair of the phenoxy group is in the right orientation for effective electronic coupling of the phenoxy and the BODIPY core and, hence, for extension of the π-system. Once the O-lone pair is delocalized over the dipyrrin ring system, merocyanine-like Lewis structures **IX** will contribute to the overall structure of **10**. The contribution to the structure of **10** of cross-conjugated Lewis structures **IX** with shorter polymethine chains than the cyanine-like Lewis structures **X** and **XI** (Figure 8) accounts for the blue shifts of the absorption and fluorescence bands of **10**. The lower electron-donating capacity of the 8-phenoxy group in **10** compared to that of 8-phenylamino and 8-benzylamino in **7** and **8**, respectively, ensures that merocyanine-like Lewis structures **IX** contributes less to the overall structure of *meso*-phenoxyBODIPY than the hemicyanine-like Lewis structures **V** to the overall structure of the *meso*-NHR substituted counterparts. This gives rise to spectra that are less hypsochromically shifted for **10** than for their 8-NHR-BODIPY counterparts **7** and **8**.

QUANTUM-CHEMICAL CALCULATIONS OF 8-AMINOBODIPYS

All the quantum-chemical calculations were performed using the Gaussian 09 package.[89] In the framework of density functional theory (DFT), ground-state geometries were fully optimized at the B3LYP/6-31G(d,p) level,[90] applying the polarizable continuum model (IEFPCM formulation[91]) to account for solvent effects (in acetonitrile). On the basis of these structures, time-dependent density functional theory (TD-DFT) has been applied to compute the vertical transition energies.

Meso-substitution of the BODIPY core can result in two sets of extreme conformations: either coplanar conformations **VIa** and **VIb** in which the BODIPY core and the *meso*-substituent are approximately in the same plane, or in a geometry that sees the two moieties in a (near-)perpendicular conformation (conformations **VII** and **VIII**), depending greatly on steric repulsion effects. These two possible arrangements lead to very different photophysical properties.

First, we investigated derivatives **12**, **13** (Chart 2), and **7** (Chart 1), which differ by the electron donor strength of the 8-NHR substituent ($-NH_2$ < $-NHPh$ < $-NHCH_3$), to evaluate the consequences on both their conformational and electronic properties.

Fully optimized ground-state geometries (Figure 9, upper row) present a coplanar-like arrangement, with dihedral angles

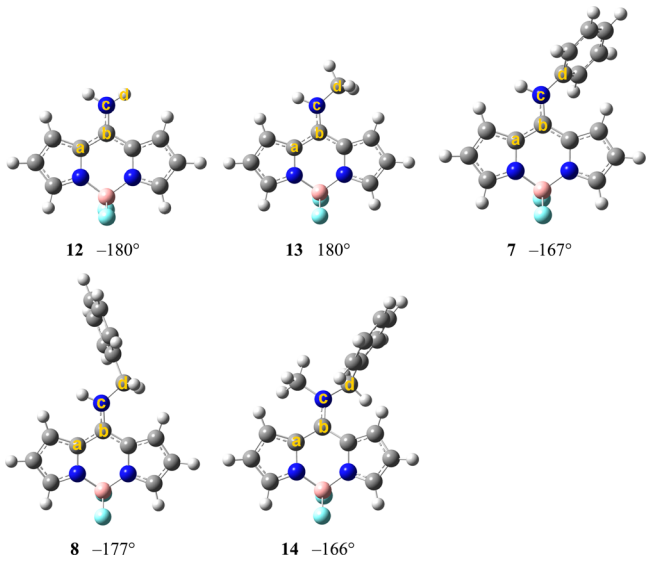

Figure 9. Optimized ground-state geometries of **12**, **13**, **7** (upper row) and **8**, **14** (lower row) and values of the associated dihedral angle between the BODIPY core and the *meso*-substituent plane, defined by atoms a, b, c, and d.

close to 180° for **12** and **13**, and a slight distortion in **7**, which exhibits a −167° angle between the two moieties, most likely as a result of the steric hindrance engendered by the larger substituent size. The conformation of the optimized ground state of **7** is in excellent agreement with the NMR spectra and X-ray data.[58]

Intuitively, one can expect that substitution by a donor group should bring about an asymmetrical destabilization of the frontier orbitals with a larger effect on the HOMO. Figures 10 and 12 present the evolution of the frontier orbitals of **12**, **13**, **7**, and **15**. Clearly, the expected trends are not observed, as the HOMO energies of **7**, **12**, and **13** are destabilized by only 0.057, 0.054, and 0.085 eV, respectively, compared to **15**, whereas the LUMOs of **7**, **12**, and **13** are destabilized by 0.548, 0.687, and 0.762 eV, respectively, in comparison with **15**. This can be rationalized considering the electronic density present at the 8-position in both orbitals. Although there is a substantial

dx.doi.org/10.1021/jp412132y | J. Phys. Chem. A 2014, 118, 1576−1594

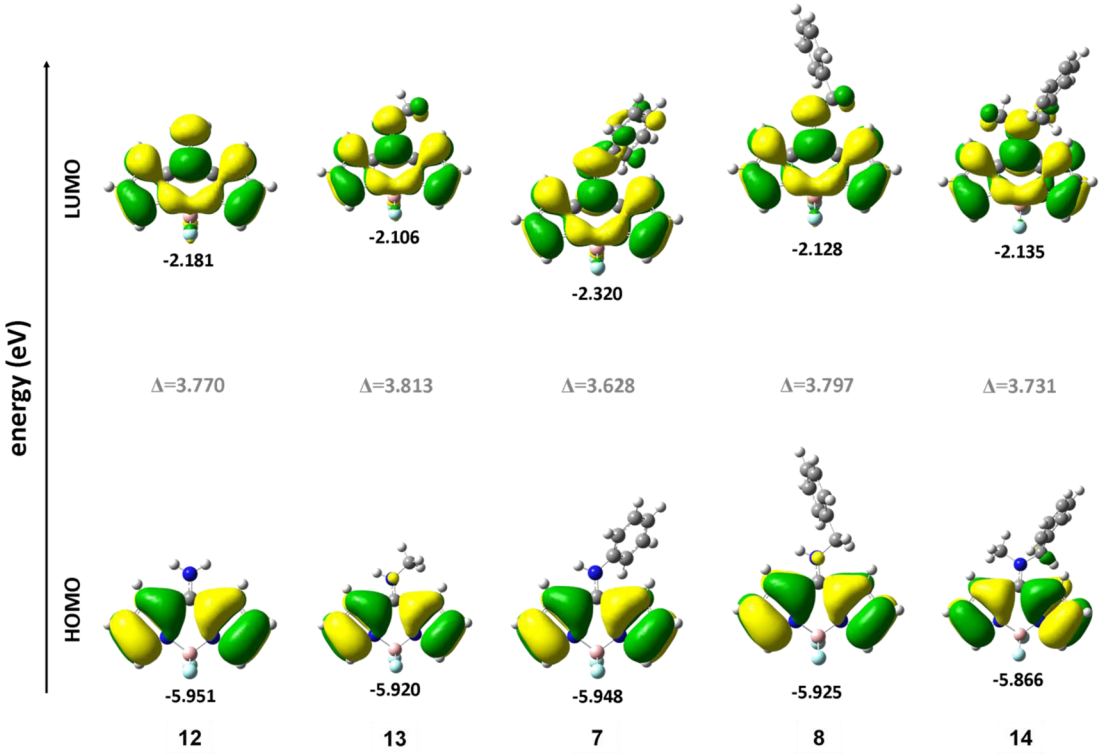

Figure 10. Graphical representation of the frontier orbitals of the compounds with their associated energy.

contribution on the N atom in the LUMO, the HOMO orbital possesses a node in its wave function at this position; hence there is no electron density on the N atom and the frontier orbitals are not equally affected by the *meso*-substitution. The N-methylation in **13** expectedly results in a very small destabilization of both frontier orbitals compared to **12**. Regarding the evolution of the LUMO orbital, it should be noted that this orbital is significantly stabilized in **7** compared to **12** and **13**, as a result of the larger delocalization which extends over the phenyl moiety. This is in line with the experimental λ_{abs}(max) and λ_{em}(max) of **7** in methanol, which are somewhat red-shifted compared to those of **12** and **13**.[60]

As expected from the relative positions of the frontier orbitals and the energy gaps between them, the smallest vertical transition energy is computed for **7** at 377 nm whereas similar but slightly higher values are obtained for **12** and **13** with transitions at 363 and 361 nm, respectively (Table 5).

Table 5. Computed Transition Wavelengths λ and Transition Energies ΔE of the First Absorption of the Compounds of Chart 2 and Their Associated Oscillator Strengths *f* with the Nature of the Transition

$S_1 \leftarrow S_0$	ΔE/eV	λ/nm	*f*	nature
12	3.42	363	0.44	HOMO → LUMO 96.9%
				HOMO−2 → LUMO 3.0%
13	3.43	361	0.41	HOMO → LUMO 96.8%
				HOMO−2 → LUMO 2.7%
7	3.29	377	0.39	HOMO → LUMO 96.7%
				HOMO−2 → LUMO 2.8%
8	3.42	363	0.39	HOMO → LUMO 96.8%
				HOMO−2 → LUMO 2.7%
14	3.30	375	0.33	HOMO → LUMO 96.5%
				HOMO−2 → LUMO 2.8%

The first absorption band is in all cases dominated by the HOMO → LUMO transition and it is thus sufficient to follow the evolution of these two orbitals to gain insight into how the photophysical properties might be affected by the nature of the 8-amino substituent and its relative positioning onto the BODIPY plane. Although the computational approach overestimates the transition energies by about 2000 to 2500 cm^{-1}, it gives the correct trend between **7** and **8**. We computed the ground-state potential energy surfaces of the three compounds **7**, **12**, and **13** as a function of the scanned dihedral angle between the chromophoric core and the 8-amino-substituent plane (Figure S9, Supporting Information).

According to the potential energy surfaces and the associated Boltzmann population histograms (Figure 11), we limit our investigations to ±50° around the fully planar, equilibrium position. The evolution of the frontier orbitals together with the corresponding HOMO−LUMO energy gap is plotted in Figure 11.

Though the HOMO is only very slightly affected by the modification of the torsion angle, the LUMO experiences a large stabilization when going from the coplanar arrangement (dihedral angle 180°) to the more perpendicular-like conformation. This evolution, which agrees with the antibonding interaction between N and C8 in the LUMO, confirms that the coplanar conformation is accompanied by a widening of the gap and should thus result in blue-shifted transitions.

For each geometry considered, the $S_1 \leftarrow S_0$ transition was also computed and its energy plotted against the dihedral angle (Figure S10, Supporting Information): its evolution is fully consistent with the trends already noticed in the HOMO−LUMO gap. Upon twisting of the *meso*-substituent, the absorption maximum is red-shifted due to a smaller destabilization of the LUMO by the electron donor moiety.

dx.doi.org/10.1021/jp412132y | J. Phys. Chem. A 2014, 118, 1576−1594

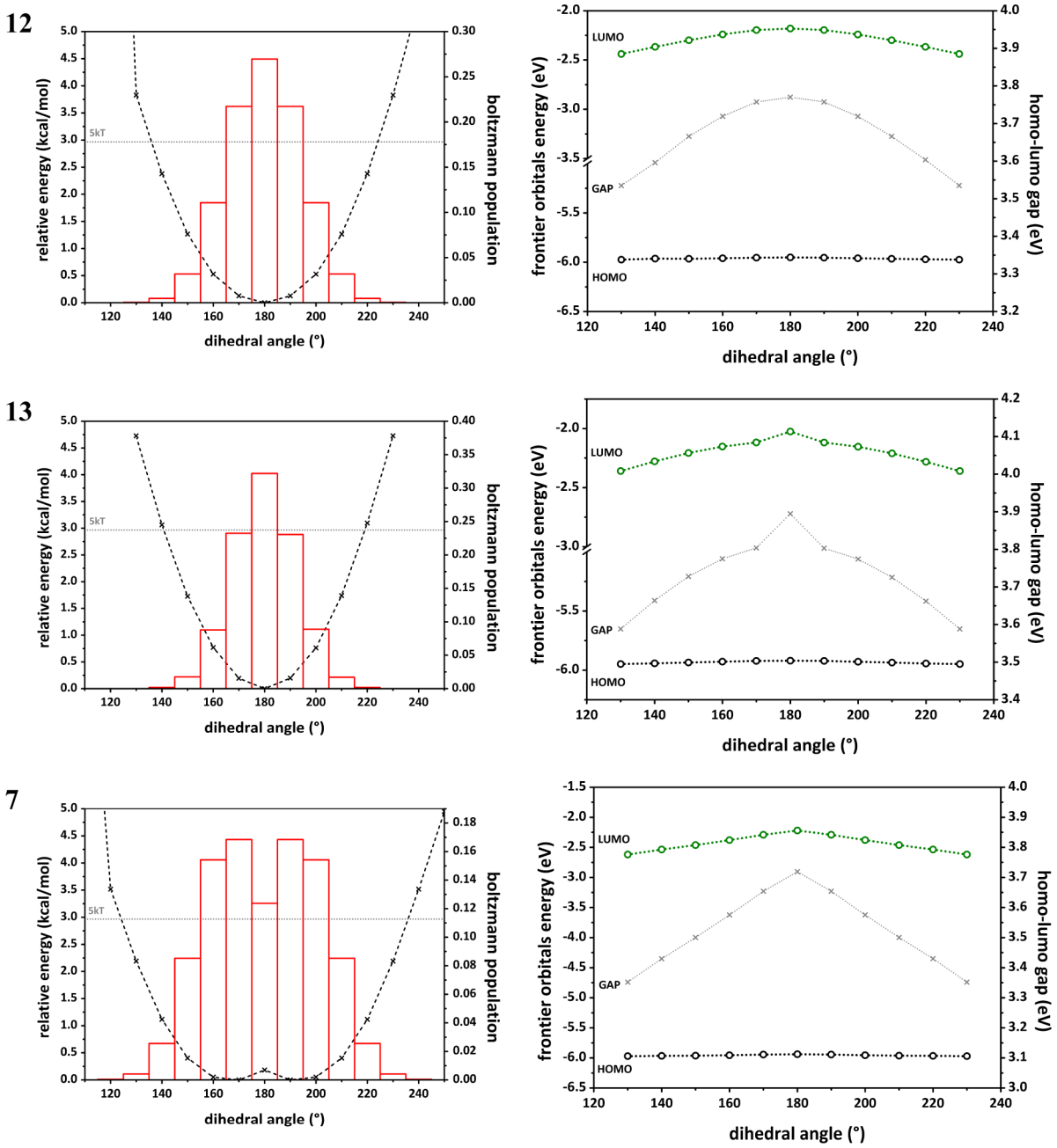

Figure 11. Individual potential energy surfaces (black) with Boltzmann population histograms (red) for **12**, **13**, and **7** and associated HOMO–LUMO evolution and energy gap (gray), as a function of the scanned dihedral angle between the BODIPY core and the *meso*-substituent plane.

Similar calculations were performed for **8** and **14**, in which the phenyl substituent is not directly linked to 8-N. The optimized geometries of **8** and **14** reveal an almost coplanar conformation of the *meso*-substituent with respect to the BODIPY core with dihedral angles of −177° and −166°, respectively (Figure 9, lower row). Hence, it is not surprising that the HOMO and LUMO energies calculated for **8** and **14** are very close to those found for **12** and **13**. Note that the most stable geometry calculated for **8** also corresponds to the structure A determined by X-ray diffraction (see above).

In **8** and **14**, the phenyl substituent is not directly linked to 8-N so that delocalization in the LUMO does not extend over the phenyl ring as in **7**, but vanishingly small weights are noticeable over the CH_2 in **8** and, in **14**, also over C1 of the phenyl ring to which it is linked (Figure 10). This is consistent with the overall frontier orbital delocalization experienced by **8** and **14**, compared to **7**. Methylation of 8-N in **14** allows for further delocalization in **14**, which most likely accounts for rather similar LUMO energies in **8**, **12**, and **14**. However, it also increases its donor character and this can be seen in the small (0.05 eV) HOMO destabilization (Figure 10) compared to **13** or **8**. The MO diagrams of Figure 10 can also rationalize the solvatochromism of **7** and **8**. Upon excitation, electron density is transferred from the BODIPY core to the *meso*-nitrogen, which corresponds to a smaller contribution of the dipolar hemicyanine-like Lewis structure **V** (Figure 3) to the excited state and hence a decrease of the permanent dipole moment upon excitation. The decreased contribution of **V** to the excited state of **7** and **8** is also suggested by the antibonding interaction

dx.doi.org/10.1021/jp412132y | J. Phys. Chem. A 2014, 118, 1576–1594

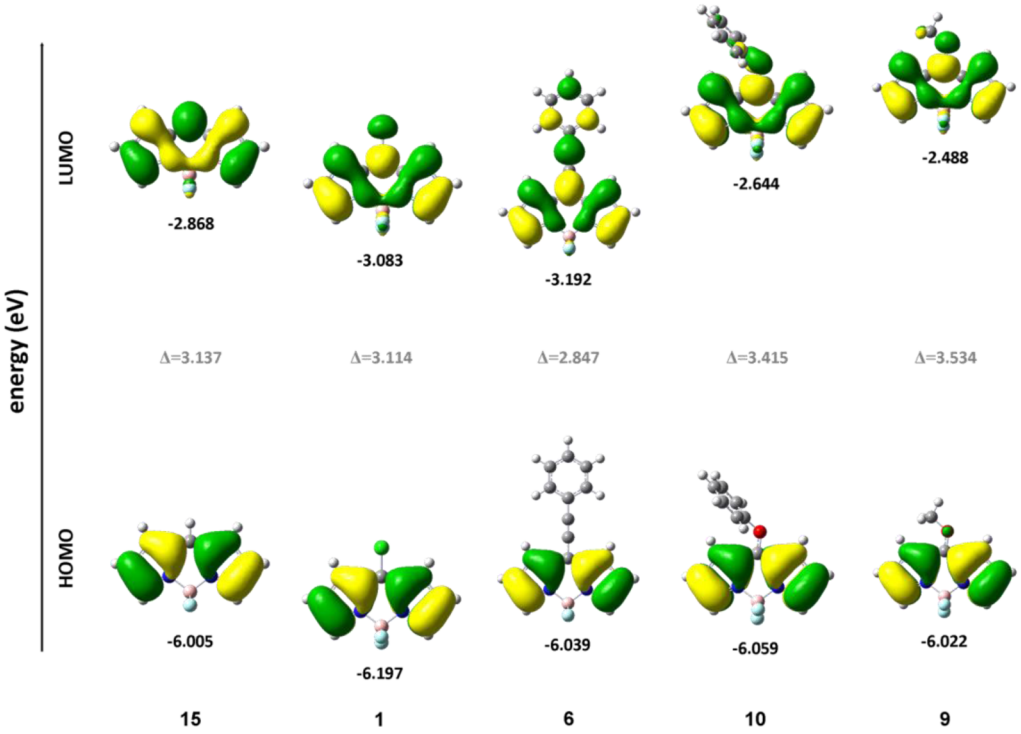

Figure 12. Graphical representation of the frontier orbitals of unsubstituted BODIPY **15** and its *meso*-substituted analogues **1**, **6**, **9**, and **10** with their associated energy.

between C8 and N in the LUMO, leading to a decrease of the double bond character between C8 and N upon excitation.

DFT CALCULATIONS ON UNSUBSTITUTED BODIPY (15) AND ITS 8-CHLORO (1), 8-(2-PHENYLETHYNYL) (6), 8-METHOXY (9), AND 8-PHENOXY (10) ANALOGUES

DFT calculations were performed on unsubstituted BODIPY **15**, its *meso*-chloro (**1**) and *meso*-alkynyl (**6**) derivatives, as well as on the *meso*-alkoxy (**9**) and *meso*-aryloxy (**10**) compounds. In line with recently reported results,[66,67,92] we rationalize the change in their optical properties as a function of the evolution of their frontier orbitals (Figure 12).

As found for the 8-aminoBODIPYs (see above), the HOMO presents a node at the *meso*-carbon and is therefore unaltered (within 0.05 eV) by the substitution in **6**, **9**, and **10** compared to the reference, i.e., unsubstituted BODIPY **15** (the stabilization by ∼0.2 eV experienced by the HOMO of **1** arises from the inductive effect exerted by the chlorine atom). Conversely, the LUMO has no node on the carbon atom in 8-position and is thus very sensitive to *meso*-substitution.

The 2-phenylethynyl group at the 8-position of **6** does not contribute to the HOMO, whose energy level is very similar to that of unsubstituted BODIPY **15**. As for the LUMO, it is delocalized over the whole molecule and, as a result, significantly stabilized by ∼0.3 eV compared to **15**. Thus a smaller HOMO−LUMO gap is obtained, which accounts for the red-shifted absorption and fluorescence spectra of **6** relative to **15**. In contrast to the 8-amino substituted BODIPYs, the interaction between C8 and the first carbon of the ethynyl group in **6** is bonding.

Due to the electron-donating effect of the 8-alkoxy group, the LUMO orbital of **9** is largely destabilized by ∼0.4 eV. Because of the node it exhibits on the central C8-position, the HOMO remains almost unaltered. The more pronounced destabilization of the LUMO compared to that of the HOMO leads to an increase in the HOMO−LUMO energy gap, thus giving rise to blue-shifted absorption and emission of **9** relative to unsubstituted **15** and 8-chloro derivative **1**.[65] This evolution is further illustrated by the coplanar arrangement of the methoxy substituent with respect to the BODIPY plane (dihedral angle of −179°), supporting the formation of the merocyanine-like Lewis structure **IX** associated with spectral hypsochromic shifts. The widening of the HOMO−LUMO energy gap depends on the electron-releasing ability of the substituent. Thus, the 8-alkoxy group has a lower electron-donating character compared to its 8-NHR counterpart and, consequently, the destabilization of the LUMO and the increase of the energy gap is lower with an 8-alkoxy than with an 8-alkylamino substituent. This results in spectra that are less blue-shifted for **9** than for the 8-NHR-BODIPY analogues. As found for the 8-amino substituted BODIPYs, the interaction between C8 and O is antibonding. The lower electron-releasing capacity of the phenoxy group in **10** compared to that of methoxy in **9** also accounts for the slightly smaller hypsochromic shifts of **10** than the shifts in **9** and related 8-alkoxy derivatives. This is confirmed by the evolution of their respective frontier orbitals: although the HOMO energies are very similar for both compounds, the LUMO level of **9** is significantly more destabilized, resulting in a larger HOMO−LUMO gap. Again, the interaction between C8 and O is antibonding.

CONCLUSIONS

We have studied the spectroscopic and photophysical properties of 8-halogenated (Cl, Br, I; **1**−**5**) difluoroboron dipyrrins and their 8-(C, N, O, S; **6**−**11**) substituted analogues. *Meso*-haloBODIPYs have narrow absorption and fluorescence

dx.doi.org/10.1021/jp412132y | J. Phys. Chem. A 2014, 118, 1576−1594

emission bands and generally quite small Stokes shifts typical of classic difluoroboron dipyrrins. Conversely, fluorophores with 8-phenylamino (**7**), 8-benzylamino (**8**), 8-methoxy (**9**), and 8-phenoxy (**10**) groups emit in the blue range of the visible spectrum and have larger Stokes shifts than familiar BODIPY dyes, whereas 8-(2-phenylethynyl)BODIPY (**6**) has red-shifted spectra compared to common BODIPYs. Quantum-chemical calculations have been performed to assess the effect of the *meso*-substituent on the spectroscopic properties. The solvent effect on $\overline{\nu}_{abs}$ and $\overline{\nu}_{em}$ of **6**, **8**, and **10** has been analyzed using the generalized Catalán solvent scales. Restricted rotation about the C8−N bond in **7** and **8** has been experimentally detected using temperature dependent ^{1}H NMR spectroscopy, whereas for **10** the rotation about the C8−O bond is not hindered. The crystal structure of **8** demonstrates that the short C8−N bond has a significant double character and that this N atom exhibits a trigonal planar geometry. In the case of **10**, the crystal structure shows a short C−O bond and an intramolecular C−H···π interaction.

■ ASSOCIATED CONTENT

Supporting Information

Experimental details on crystal structure determination, time-resolved fluorescence measurements, and relative fluorescence quantum yield determinations. Solvatochromic analysis of absorption and fluorescence maxima. Fluorescence decay histograms. VT ^{1}H NMR spectra of **7**, ^{1}H COSY NMR of **8** in $CDCl_3$, ^{1}H NMR of **8** in DMSO. Calculated potential energy surfaces and transition energies of **7**, **12**, and **13**. Crystallographic data for **7**, **8**, and **10**. This material is available free of charge via the Internet at http://pubs.acs.org.

■ AUTHOR INFORMATION

Corresponding Author

*N. Boens: e-mail, Noel.Boens@chem.kuleuven.be; tel, +32-16-327497; fax, +32-16-327990.

Present Addresses

[‖]College of Environment and Safety Engineering, Qingdao University of Science and Technology, Qingdao, Shandong province 266042, China.

[⊥]Department of Chemistry, Yale University, New Haven, CT 06520, United States.

Notes

The authors declare no competing financial interest.

■ ACKNOWLEDGMENTS

The collaboration between Leuven and Mons is supported by the Science Policy Office of the Belgian Federal Government (BELSPO-IAP). Research in Mons is also supported by FNRS/FRFC and Région Wallonne (Programme d'excellence OPTI2-MAT). D. Beljonne is a Research Director of the Fonds National de la Recherche Scientifique (FNRS, Belgium). L. Van Meervelt and J. Jacobs from KU Leuven thank the Hercules Foundation for supporting the purchase of the diffractometer through project AKUL/09/0035.

■ REFERENCES

(1) Treibs, A.; Kreuzer, F.-H. Difluorboryl-Komplexe von Di- und Tripyrrylmethenen. *Liebigs Ann. Chem.* **1968**, *718*, 208−223.

(2) Loudet, A.; Burgess, K. BODIPY Dyes and Their Derivatives: Syntheses and Spectroscopic Properties. *Chem. Rev.* **2007**, *107*, 4891−4932.

(3) Ulrich, G.; Ziessel, R.; Harriman, A. The Chemistry of Fluorescent BODIPY Dyes: Versatility Unsurpassed. *Angew. Chem., Int. Ed.* **2008**, *47*, 1184−1201.

(4) Haugland, R. P. *The Handbook. A guide to fluorescent probes and labeling technologies*, 10th ed.; Invitrogen: Eugene, OR, 2005.

(5) Boens, N.; Leen, V.; Dehaen, W. Fluorescent Indicators Based on BODIPY. *Chem. Soc. Rev.* **2012**, *41*, 1130−1172.

(6) Boens, N.; Qin, W.; Baruah, M.; De Borggraeve, W. M.; Filarowski, A.; Smisdom, N.; Ameloot, M.; Crovetto, L.; Talavera, E. M.; Alvarez-Pez, J. M. Rational Design and Spectroscopic Properties of a Visible Light Excitable, Ratiometric, Brightly Fluorescent, Near-Neutral pH Indicator Based on the BODIPY Fluorophore. *Chem.—Eur. J.* **2011**, *17*, 10924−10934.

(7) López Arbeloa, F.; Bañuelos, J.; Martinez, V.; Arbeloa, T.; López Arbeloa, I. Structural, photophysical and lasing properties of pyrromethene dyes. *Int. Rev. Phys. Chem.* **2005**, *24*, 339−374.

(8) Ortiz, M. J.; García-Moreno, I.; Agarrabeitia, A. R.; Duran-Sampedro, G.; Costela, A.; Sastre, R.; López Arbeloa, F.; Bañuelos Prieto, J.; López Arbeloa, I. Red-Edge-Wavelength Finely-Tunable Laser Action from New BODIPY Dyes. *Phys. Chem. Chem. Phys.* **2010**, *12*, 7804−7811.

(9) Benstead, M.; Mehl, G. H.; Boyle, R. W. 4,4′-Difluoro-4-bora-3a,4a-diaza-*s*-indacenes (BODIPYs) as Components of Novel Light Active Materials. *Tetrahedron* **2011**, *67*, 3573−3601.

(10) Kamkaew, A.; Lim, S. H.; Lee, H. B.; Kiew, L. V.; Chung, L. Y.; Burgess, K. BODIPY Dyes in Photodynamic Therapy. *Chem. Soc. Rev.* **2013**, *42*, 77−88.

(11) Wan, C.-W.; Burghart, A.; Chen, J.; Bergström, F.; Johansson, L. B.-Å.; Wolford, M. F.; Kim, T. G.; Topp, M. R.; Hochstrasser, R. M.; Burgess, K. Anthracene−BODIPY Cassettes: Syntheses and Energy Transfer. *Chem.—Eur. J.* **2003**, *9*, 4430−4441.

(12) Ziessel, R.; Goze, C.; Ulrich, G.; Césario, M.; Retailleau, P.; Harriman, A.; Rostron, J. P. Intramolecular Energy Transfer in Pyrene−BODIPY Molecular Dyads and Triads. *Chem.—Eur. J.* **2005**, *11*, 7366−7378.

(13) Yilmaz, M. D.; Bozdemir, O. A.; Akkaya, E. U. Light Harvesting and Efficient Energy Transfer in a Boron-dipyrrin (BODIPY) Functionalized Perylenediimide Derivative. *Org. Lett.* **2006**, *8*, 2871−2873.

(14) Harriman, A.; Izzet, G.; Ziessel, R. Rapid Energy Transfer in Cascade-Type BODIPY Dyes. *J. Am. Chem. Soc.* **2006**, *128*, 10868−10875.

(15) Liu, J.-Y.; Yeung, H.-S.; Xu, W.; Li, X.; Ng, D. K. P. Highly Efficient Energy Transfer in Subphthalocyanine−BODIPY Conjugates. *Org. Lett.* **2008**, *10*, 5421−5424.

(16) Ziessel, R.; Ulrich, G.; Elliott, K. J.; Harriman, A. Electronic Energy Transfer in Molecular Dyads Built Around Boron−Ethyne-Substituted Subphthalocyanines. *Chem.—Eur. J.* **2009**, *15*, 4980−4984.

(17) Barin, G.; Yilmaz, M. D.; Akkaya, E. U. Boradiazaindacene (BODIPY)-based building blocks for the construction of energy transfer cassettes. *Tetrahedron Lett.* **2009**, *50*, 1738−1740.

(18) Yin, S.; Leen, V.; Jackers, C.; Beljonne, D.; Van Averbeke, B.; Van der Auweraer, M.; Boens, N.; Dehaen, W. Oligo (*p*-phenylene ethynylene)−BODIPY Derivatives: Synthesis, Energy Transfer, and Quantum-Chemical Calculations. *Chem.—Eur. J.* **2011**, *17*, 13247−13257.

(19) Ueno, Y.; Jose, J.; Loudet, A.; Pérez-Bolívar, C.; Anzenbacher, P., Jr.; Burgess, K. Encapsulated Energy-Transfer Cassettes with Extremely Well Resolved Fluorescent Outputs. *J. Am. Chem. Soc.* **2011**, *133*, 51−55.

(20) Yu, H.; Xiao, Y.; Guo, H.; Qian, X. Convenient and Efficient FRET Platform Featuring a Rigid Biphenyl Spacer between Rhodamine and BODIPY: Transformation of 'Turn-On' Sensors into Ratiometric Ones with Dual Emission. *Chem.—Eur. J.* **2011**, *17*, 3179−3191.

(21) Bai, D.; Benniston, A. C.; Hagon, J.; Lemmetyinen, H.; Tkachenko, N. V.; Clegg, W.; Harrington, R. W. Exploring Förster Electronic Energy Transfer in a Decoupled Anthracenyl-Based

Borondipyrromethene (BODIPY) Dyad. *Phys. Chem. Chem. Phys.* **2012**, *14*, 4447−4456.
(22) Khan, T. K.; Shaikh, M. S.; Ravikanth, M. Synthesis and photophysical properties of covalently linked boron dipyrromethene dyads. *Dyes Pigm.* **2012**, *94*, 66−73.
(23) Hattori, S.; Ohkubo, K.; Urano, Y.; Sunahara, H.; Nagano, T.; Wada, Y.; Tkachenko, N. V.; Lemmetyinen, H.; Fukuzumi, S. Charge Separation in a Nonfluorescent Donor−Acceptor Dyad Derived from Boron Dipyrromethene Dye, Leading to Photocurrent Generation. *J. Phys. Chem. B.* **2005**, *109*, 15368−15375.
(24) Erten-Ela, S.; Yilmaz, M. D.; Icli, B.; Dede, Y.; Icli, S.; Akkaya, E. U. A Panchromatic Boradiazaindacene (BODIPY) Sensitizer for Dye-Sensitized Solar Cells. *Org. Lett.* **2008**, *10*, 3299−3302.
(25) Kumaresan, D.; Thummel, R. P.; Bura, T.; Ulrich, G.; Ziessel, R. Color Tuning in New Metal-Free Organic Sensitizers (BODIPYs) for Dye-Sensitized Solar Cells. *Chem.—Eur. J.* **2009**, *15*, 6335−6339.
(26) Lee, C. Y.; Hupp, J. T. Dye Sensitized Solar Cells: TiO_2 Sensitization with a BODIPY-Porphyrin Antenna System. *Langmuir* **2010**, *26*, 3760−3765.
(27) Kolemen, S.; Bozdemir, O.; Cakmak, A. Y.; Barin, G.; Erten-Ela, S.; Marszalek, M.; Yum, J.-H.; Zakeeruddin, S. M.; Nazeeruddin, M. K.; Grätzel, M.; et al. Optimization of Distyryl-BODIPY Chromophores for Efficient Panchromatic Sensitization in Dye Sensitized Solar Cells. *Chem. Sci.* **2011**, *2*, 949−954.
(28) Warnan, J.; Buchet, F.; Pellegrin, Y.; Blart, E.; Odobel, F. Panchromatic Trichromophoric Sensitizer for Dye-Sensitized Solar Cells Using Antenna Effect. *Org. Lett.* **2011**, *13*, 3944−3947.
(29) Bozdemir, O. A.; Erbas-Cakmak, S.; Ekiz, O. O.; Dana, A.; Akkaya, E. U. Towards Unimolecular Luminescent Solar Concentrators: BODIPY-Based Dendritic Energy-Transfer Cascade with Panchromatic Absorption and Monochromatized Emission. *Angew. Chem., Int. Ed.* **2011**, *50*, 10907−10912.
(30) Leen, V.; Yuan, P.; Wang, L.; Boens, N.; Dehaen, W. Synthesis of *Meso*-Halogenated BODIPYs and Access to *Meso*-Substituted Analogues. *Org. Lett.* **2012**, *14*, 6150−6153.
(31) Catalán, J. Toward a Generalized Treatment of the Solvent Effect Based on Four Empirical Scales: Dipolarity (SdP, a New Scale), Polarizability (SP), Acidity (SA), and Basicity (SB) of the Medium. *J. Phys. Chem. B* **2009**, *113*, 5951−5960.
(32) Qin, W.; Baruah, M.; Van der Auweraer, M.; De Schryver, F. C.; Boens, N. Photophysical Properties of Borondipyrromethene Analogues in Solution. *J. Phys. Chem. A* **2005**, *109*, 7371−7384.
(33) Qin, W.; Baruah, M.; Stefan, A.; Van der Auweraer, M.; Boens, N. Photophysical Properties of BODIPY-Derived Hydroxyaryl Fluorescent pH Probes in Solution. *ChemPhysChem* **2005**, *6*, 2343−2351.
(34) Qin, W.; Rohand, T.; Baruah, M.; Dehaen, W.; Stefan, A.; Van der Auweraer, M.; Boens, N. Solvent-Dependent Photophysical Properties of Borondipyrromethene Dyes in Solution. *Chem. Phys. Lett.* **2006**, *420*, 562−568.
(35) Qin, W.; Rohand, T.; Dehaen, W.; Clifford, J. N.; Driesen, K.; Beljonne, D.; Van Averbeke, B.; Van der Auweraer, M.; Boens, N. Boron Dipyrromethene Analogs with Phenyl, Styryl, and Ethynylphenyl Substituents: Synthesis, Photophysics, Electrochemistry, and Quantum-Chemical Calculations. *J. Phys. Chem. A* **2007**, *111*, 8588−8597.
(36) Rohand, T.; Lycoops, J.; Smout, S.; Braeken, E.; Sliwa, M.; Van der Auweraer, M.; Dehaen, W.; De Borggraeve, W. M.; Boens, N. Photophysics of 3,5-diphenoxy substituted BODIPY Dyes in Solution. *Photochem. Photobiol. Sci.* **2007**, *6*, 1061−1066.
(37) Leen, V.; Qin, W.; Yang, W.; Cui, J.; Xu, C.; Tang, X.; Liu, W.; Robeyns, K.; Van Meervelt, L.; Beljonne, D.; et al. Synthesis, Spectroscopy, Crystal Structure Determination, and Quantum Chemical Calculations of BODIPY Dyes with Increasing Conformational Restriction and Concomitant Red-Shifted Visible Absorption and Fluorescence Spectra. *Chem. Asian J.* **2010**, *5*, 2016−2026.
(38) Filarowski, A.; Kluba, M.; Cieślik-Boczula, K.; Koll, A.; Kochel, A.; Pandey, L.; De Borggraeve, W. M.; Van der Auweraer, M.; Catalán, J.; Boens, N. Generalized Solvent Scales as a Tool for Investigating Solvent Dependence of Spectroscopic and Kinetic Parameters. Application to Fluorescent BODIPY Dyes. *Photochem. Photobiol. Sci.* **2010**, *9*, 996−1008.
(39) Leen, V.; Leemans, T.; Boens, N.; Dehaen, W. 2- and 3-Monohalogenated BODIPY Dyes and Their Functionalized Analogues: Synthesis and Spectroscopy. *Eur. J. Org. Chem.* **2011**, 4386−4396.
(40) Boens, N.; Leen, V.; Dehaen, W.; Wang, L.; Robeyns, K.; Qin, W.; Tang, X.; Beljonne, D.; Tonnelé, C.; Paredes, J. M.; et al. Visible Absorption and Fluorescence Spectroscopy of Conformationally Constrained, Annulated BODIPY Dyes. *J. Phys. Chem. A* **2012**, *116*, 9621−9631.
(41) Wang, L.; Verbelen, B.; Tonnelé, C.; Beljonne, D.; Lazzaroni, R.; Leen, V.; Dehaen, W.; Boens, N. UV−Vis Spectroscopy of the Coupling Products of the Palladium-Catalyzed C−H Arylation of the BODIPY Core. *Photochem. Photobiol. Sci.* **2013**, *12*, 835−847.
(42) Vos de Wael, E.; Pardoen, J. A.; van Koeveringe, J. A.; Lugtenburg, J. Pyrromethene-BF_2 complexes (4,4′-difluoro-4-bora-3a,4a-diaza-*s*-indacenes). Synthesis and luminescence properties. *Recl. Trav. Chim. Pays-Bas* **1977**, *96*, 306−309.
(43) Karolin, J.; Johansson, L. B.-Å.; Strandberg, L.; Ny, T. Fluorescence and Absorption Spectroscopic Properties of Dipyrrometheneboron Difluoride (BODIPY) Derivatives in Liquids, Lipid Membranes, and Proteins. *J. Am. Chem. Soc.* **1994**, *116*, 7801−7806.
(44) Kollmannsberger, M.; Rurack, K.; Resch-Genger, U.; Daub, J. Ultrafast Charge Transfer in Amino-Substituted Boron Dipyrromethene Dyes and Its Inhibition by Cation Complexation: A New Design Concept for Highly Sensitive Fluorescent Probes. *J. Phys. Chem. A* **1998**, *102*, 10211−10220.
(45) Rurack, K.; Kollmannsberger, M.; Daub, J. A Highly Efficient Sensor Molecule Emitting in the Near Infrared (NIR): 3,5-distyryl-8-(*p*-dimethylaminophenyl)difluoroboradiaza-*s*-indacene. *New. J. Chem.* **2001**, *25*, 289−292.
(46) Rurack, K.; Kollmannsberger, M.; Daub, J. Molecular Switching in the Near Infrared (NIR) with a Functionalized Boron−Dipyrromethene Dye. *Angew. Chem., Int. Ed.* **2001**, *40*, 385−387.
(47) Bergström, F.; Mikhalyov, I.; Hägglöf, P.; Wortmann, R.; Ny, T.; Johansson, L. B.-Å. Dimers of Dipyrrometheneboron Difluoride (BODIPY) with Light Spectroscopic Applications in Chemistry and Biology. *J. Am. Chem. Soc.* **2002**, *124*, 196−204.
(48) Costela, A.; García-Moreno, I.; Gomez, C.; Sastre, R.; Amat-Guerri, F.; Liras, M.; López Arbeloa, F.; Bañuelos Prieto, J.; López Arbeloa, I. Photophysical and Lasing Properties of New Analogs of the Boron−Dipyrromethene Laser Dye PM567 in Liquid Solution. *J. Phys. Chem. A* **2002**, *106*, 7736−7742.
(49) Bañuelos Prieto, J.; López Arbeloa, F.; Martínez Martínez, V.; Arbeloa López, T.; Amat-Guerri, F.; Liras, M.; López Arbeloa, I. Photophysical properties of a new 8-phenyl analogue of the laser dye PM567 in different solvents: internal conversion mechanisms. *Chem. Phys. Lett.* **2004**, *385*, 29−35.
(50) Dost, Z.; Atilgan, S.; Akkaya, E. U. Distyryl-boradiazaindacenes: facile synthesis of novel near IR emitting fluorophores. *Tetrahedron* **2006**, *62*, 8484−8488.
(51) Li, Z.; Bittman, R. Synthesis and Spectral Properties of Cholesterol- and FTY720-Containing Boron Dipyrromethene Dyes. *J. Org. Chem.* **2007**, *72*, 8376−8382.
(52) Ekmekci, Z.; Yilmaz, M. D.; Akkaya, E. U. A Monostyryl-boradiazaindacene (BODIPY) Derivative as Colorimetric and Fluorescent Probe for Cyanide Ions. *Org. Lett.* **2008**, *10*, 461−464.
(53) Li, L.; Han, J.; Nguyen, B.; Burgess, K. Syntheses and Spectral Properties of Functionalized, Water-Soluble BODIPY Derivatives. *J. Org. Chem.* **2008**, *73*, 1963−1970.
(54) Jiao, L.; Yu, C.; Li, J.; Wang, Z.; Wu, M.; Hao, E. *β*-Formyl-BODIPYs from the Vilsmeier−Haack Reaction. *J. Org. Chem.* **2009**, *74*, 7525−7528.
(55) Jiao, L.; Pang, W.; Zhou, J.; Wei, Y.; Mu, X.; Bai, G.; Hao, E. Regioselective Stepwise Bromination of Boron Dipyrromethene (BODIPY) Dyes. *J. Org. Chem.* **2011**, *76*, 9988−9996.

(56) Tram, K.; Yan, H.; Jenkins, H. A.; Vassiliev, S.; Bruce, D. The Synthesis and Crystal Structure of Unsubstituted 4,4-difluoro-4-bora-3a,4a-diaza-*s*-indacene (BODIPY). *Dyes Pigm.* **2009**, *82*, 392−395.
(57) Schmitt, A.; Hinkeldey, B.; Wild, M.; Jung, G. Synthesis of the Core Compound of the BODIPY Dye Class: 4,4′-Difluoro-4-bora-(3a,4a)-diaza-*s*-indacene. *J. Fluoresc.* **2009**, *19*, 755−758.
(58) Goud, T. V.; Tutar, A.; Biellmann, J.-F. Synthesis of 8-heteroatom-substituted 4,4-difluoro-4-bora-3a,4a-diaza-*s*-indacene Dyes (BODIPY). *Tetrahedron* **2006**, *62*, 5084−5091.
(59) Gómez-Durán, C. F. A.; García-Moreno, I.; Costela, A.; Martín, V.; Sastre, R.; Bañuelos, J.; López. Arbeloa, F.; López Arbeloa, I.; Peña-Cabrera, E. 8-PropargylaminoBODIPY: Unprecedented Blue-Emitting Pyrromethene Dye. Synthesis, Photophysics and Laser Properties. *Chem. Commun.* **2010**, *46*, 5103−5105.
(60) Bañuelos, J.; Martín, V.; Gómez-Durán, C. F. A.; Arroyo Córdoba, I. J.; Peña-Cabrera, E.; García-Moreno, I.; Costela, A.; Pérez-Ojeda, M. E.; Arbeloa, T.; López Arbeloa, I. New 8-Amino-BODIPY Derivatives: Surpassing Laser Dyes at Blue-Edge Wavelengths. *Chem.—Eur. J.* **2011**, *17*, 7261−7270.
(61) Osorio-Martínez, C. A.; Urías-Benavides, A.; Gómez-Durán, C. F. A.; Bañuelos, J.; Esnal, I.; López Arbeloa, I.; Peña-Cabrera, E. 8-AminoBODIPYs: Cyanines or Hemicyanines? The Effect of the Coplanarity of the Amino Group on Their Optical Properties. *J. Org. Chem.* **2012**, *77*, 5434−5438.
(62) Roacho, R. I.; Metta-Magaña, A.; Portillo, M. M.; Peña-Cabrera, E.; Pannell, K. H. 8-Amino-BODIPYs: Structural Variation, Solvent-Dependent Emission, and VT NMR Spectroscopic Properties of 8-R_2N-BODIPY. *J. Org. Chem.* **2013**, *78*, 4245−4250.
(63) Kölle, P. Ultrafast Emission Quenching in Perylene Diimides by Structure Rearrangement Induced Electron Transfer from their Substituents. In *Book of Abstracts ICP*; Roeffaers, M.; Hofkens, J., Eds.; Department of Chemistry, Faculty of Science, KU Leuven: Leuven, Belgium, 2013; p 185.
(64) Kim, D.; Yamamoto, K.; Ahn, K. H. A BODIPY-Based Reactive Probe for Ratiometric Fluorescence Sensing of Mercury Ions. *Tetrahedron* **2012**, *68*, 5279−5282.
(65) Wang, L.; Zhang, Y.; Xiao, Y. *meso*-Alkoxy BODIPYs with a Good Balance between Larger Stokes Shifts and Higher Fluorescence Quantum Yields. *RSC Adv.* **2013**, *3*, 2203−2206.
(66) Flores-Rizo, J. O.; Esnal, I.; Osorio-Martínez, C. A.; Gómez-Durán, C. F. A.; Bañuelos, J.; López Arbeloa, I.; Pannell, K. H.; Metta-Magaña, A. J.; Peña-Cabrera, E. 8-Alkoxy- and 8-Aryloxy-BODIPYs: Straightforward Fluorescent Tagging of Alcohols and Phenols. *J. Org. Chem.* **2013**, *78*, 5867−5877.
(67) Kusaka, S.; Sakamoto, R.; Kitagawa, Y.; Okumura, M.; Nishihara, H. *meso*-Alkynyl BODIPYs: Structure, Photoproperties, π-Extension, and Manipulation of Frontier Orbitals. *Chem. Asian. J.* **2013**, *8*, 723−727.
(68) Misra, R.; Dhokale, B.; Jadhav, T.; Mobin, S. M. Donor−Acceptor *meso*-Alkynylated Ferrocenyl BODIPYs: Synthesis, Structure, and Properties. *Dalton Trans.* **2013**, *42*, 13658−13666.
(69) Bonardi, L.; Ulrich, G.; Ziessel, R. Tailoring the Properties of Boron−Dipyrromethene Dyes with Acetylenic Functions at the 2,6,8 and 4-B Substitution Positions. *Org. Lett.* **2008**, *10*, 2183−2186.
(70) Gräf, K.; Körzdörfer, T.; Kümmel, S.; Thelakkat, M. Synthesis of Donor-Substituted *meso*-Phenyl and *meso*-Ethynylphenyl BODIPYs with Broad Absorption. *New J. Chem.* **2013**, *37*, 1417−1426.
(71) Acebal, P.; Blaya, S.; Carretero, L. Dipyrromethene−BF_2 Complexes with Optimized Electrooptic Properties. *Chem. Phys. Lett.* **2003**, *382*, 489−495.
(72) Braslavsky, S. E. Glossary of Terms Used in Photochemistry, 3rd ed.; IUPAC Recommendations 2006. *Pure Appl. Chem.* **2007**, *79*, 293−465.
(73) Lavis, L. D.; Raines, R. T. Bright Ideas for Chemical Biology. *ACS Chem. Biol.* **2008**, *3*, 142−155.
(74) Becker, W. *Advanced time-correlated single photon counting techniques*; Springer Series in Chemical Physics, Vol. *81*, Springer: Berlin, 2005.
(75) vandeVen, M.; Ameloot, M.; Valeur, B.; Boens, N. Pitfalls and Their Remedies in Time-Resolved Fluorescence Spectroscopy and Microscopy. *J. Fluoresc.* **2005**, *15*, 377−413.
(76) Boens, N.; Qin, W.; Basarić, N.; Hofkens, J.; Ameloot, M.; Pouget, J.; Lefèvre, J. P.; Valeur, B.; Gratton, E.; Vandeven, M.; et al. Fluorescence Lifetime Standards for Time and Frequency Domain Fluorescence Spectroscopy. *Anal. Chem.* **2007**, *79*, 2137−2149.
(77) Catalán, J.; Hopf, H. Empirical Treatment of the Inductive and Dispersive Components of Solute−Solvent Interactions: The Solvent Polarizability (SP) Scale. *Eur. J. Org. Chem.* **2004**, 4694−4702.
(78) Catalán, J. In *Handbook of solvents*; Wypych, G., Ed.; ChemTec Publishing: Toronto, 2001; pp 583−616.
(79) Catalán, J.; Díaz, C. A Generalized Solvent Acidity Scale: The Solvatochromism of *o*-*tert*-Butylstilbazolium Betaine Dye and Its Homomorph *o*,*o*′-Di-*tert*-butylstilbazolium Betaine Dye. *Liebigs Ann.* **1997**, 1941−1949.
(80) Catalán, J.; Díaz, C.; López, V.; Pérez, P.; de Paz, J. L. G.; Rodriguez, J. G. A Generalized Solvent Basicity Scale: The Solvatochromism of 5-Nitroindoline and Its Homomorph 1-Methyl-5-nitroindoline. *Liebigs Ann.* **1996**, 1785−1794.
(81) Kuhn, H.; Huber, W.; Handschig, G.; Martin, H.; Schäfer, F.; Bär, F. Nature of the Free Electron Model. The Simple Case of the Symmetric Polymethines. *J. Chem. Phys.* **1960**, *32*, 467−469.
(82) Kuhn, H. Elektronengasmodell zur quantitativen Deutung der Lichtabsorption von organischen Farbstoffen II. Teil B. Störung des Elektronengases durch Heteroatome. *Helv. Chim. Acta* **1951**, *34*, 2371−2402.
(83) Kuhn, H.; Försterling, H.-D. *Principles of Physical Chemistry*; Wiley: Chichester, U.K., 2000; pp 211−213.
(84) Brooker, L. G. S.; White, F. L.; Keyes, G. H. J.; Smyth, C. P.; Oesper, P. F. Color and Constitution. II. Absorptions of Some Related Vinylene-Homologous Series. *J. Am. Chem. Soc.* **1941**, *63*, 3192−3203.
(85) Brooker, L. G. S.; Keyes, G. H. J.; Williams, W. W. Color and Constitution. V. The Absorption of Unsymmetrical Cyanines. Resonance as a Basis for a Classification of Dyes. *J. Am. Chem. Soc.* **1942**, *64*, 199−210.
(86) Hamer, F. M. *The Cyanine Dyes and Related Compounds*; Interscience Publishers, John Wiley: New York, 1964.
(87) Brooker, L. G. S.; Keyes, G. H.; Sprague, R. H.; Van Dyke, R. H.; Van Lare, E.; Vanzandt, G.; White, F. L.; Cressman, H. W.; Dent, S. G. Studies in the Cyanine Dye Series. XI. The Merocyanines. *J. Am. Chem. Soc.* **1951**, *73*, 5326−5332.
(88) Friebolin, H. *Basic One- and Two-Dimensional NMR Spectroscopy*, 5th ed.; Wiley-VCH: Weinheim, Germany, 2011.
(89) Frisch, M. J.; Trucks, G. W.; Schlegel, H. B.; Scuseria, G. E.; Robb, M. A.; Cheeseman, J. R.; Scalmani, G.; Barone, V.; Mennucci, B.; Petersson, G. A.; et al. *Gaussian 09*, Revision B.01 and C.01; Gaussian, Inc.; Wallingford, CT, 2009.
(90) Becke, A. D. Completely Numerical Calculations on Diatomic Molecules in the Local-Density Approximation. *Phys. Rev. A* **1986**, *33*, 2786−2788.
(91) Mennucci, B.; Cancès, E.; Tomasi, J. Evaluation of Solvent Effects in Isotropic and Anisotropic Dielectrics and in Ionic Solutions with a Unified Integral Equation Method: Theoretical Bases, Computational Implementation, and Numerical Applications. *J. Phys. Chem. B* **1997**, *101*, 10506−10517.
(92) Briggs, E. A.; Besley, N. A.; Robinson, D. QM/MM Excited State Molecular Dynamics and Fluorescence Spectroscopy of BODIPY. *J. Phys. Chem. A* **2013**, *117*, 2644−2650.